Doctoral thesis

Molecular mechanisms underlying the skin and its appendage's appearance affected by dermal mesenchymal cells

（真皮間葉系細胞が皮膚及び付属器の外観に及ぼす影響の分子機構）

The United Graduate School of Veterinary Science
Yamaguchi University

Yuzo YOSHIDA

March 2020

CONTENTS

List of tables and figures

CHAPTER I

CHAPTER II

Abbreviations

DP; dermal papilla

DS; dermal sheath

DSC; dermal sheath cup

DF(s); dermal fibroblast(s)

EGFP; enhanced green fluorescent protein

FBS; fetal bovine serum

HGF; hepatocyte growth factor

HEK: human epidermal keratinocytes

HMVEC; human microvascular endothelial cells

LCM; laser capture microdissection

PDGFR-beta; platelet-derived growth factor receptor-beta

qRT-PCR; quantitative real-time reverse transcription-polymerase chain reaction

S.D.; standard deviation

SEM; standard error of the mean

UV; ultraviolet

2D; two dimensional

3D: three dimensional

CHAPTER I: General introduction

CHAPTER I: General introduction

I.1 The history of dermatology

Skin is a large and essential organ in the human body. Human skin, composed of both epidermis and dermis, comprises 5.5% of the total body weight of an average male (70 kg) [1]. If subcutaneous fat located in the hypodermal area is also considered to be skin then human skin could be considered to be the largest organ in the human body by weight, discussed in a previous report [2]. The major role of skin is to act as a physical barrier that protects the body from external substances and regulates fluid balance.

Characteristic changes in skin appearance can represent clinical symptoms of disease. Dermatology, and dermatological research, begun from the observation that human skin rashes have characteristic appearances and textures. Although there are still conflicts, modern dermatology is thought to have originated from the work of the Austrian military surgeon, Joseph Jacob Ritter con Plenck (1738-1807), who wrote a latin textbook entitled "Doctrina de morbis cutaneis" (teaching on the diseases of the skin) that was published in 1776. In the book, Plenck classifies skin diseases into 14 categories, based on characteristic clinical appearance [3, 4]. In 1808, the English physician Robert Willan (1757-1812) published "On Cutaneous Diseases, volume 1". In this book, Willan defined 10 skin lesions in detail, and classified skin diseases into 8 categories based on clinical

appearance, taking Plenck's classifications into account [3, 5]. Some terms defined in this textbook are still familiar to dermatologists today. These books and their works are considered to be the basics of modern dermatology. Their precise clinical observations of skin appearances have been crucial to the systematic understanding of skin disease. In addition, histopathological studies have been also critical in the definition of characteristic symptoms, observed especially in the internal part of skin. Finally, histological studies have also been central to the investigation of the structure of skin and these will be described in the next chapter.

I.2 The histological structure of skin

Skin is composed of epidermis and dermis, and subcutaneous tissue is located in the hypodermal area (Fig. 1-1). Epidermis is the superficial layer of skin (Fig. 1-1), which is further composed of stratum corneum, granular cell layer, prickle cell layer and basal cell layer from superficial to deep, respectively. Epidermis is maintained by epidermal stem cells and their derived transit-amplifying cells located in the basal layer. Transit-amplifying cells proliferate and occupy the basal layer, and then differentiate into prickle cells, followed by differentiation to granular cells, which undergo further terminal differentiation to form the stratum corneum layer. These differentiation process occur

when the cell is relocating from the basal to the superficial skin layer. In human skin, the epidermal turnover time is 39 days, based on the assessment of proliferation properties of epidermal cells incorporating tritiated thymidine with autoradiographic technique [6]. At the boundary between the epidermis and dermis skin layers, undulated rete ridge structure is observed, which is flattening with aging in humans [7].

The major role of skin and superficial epidermis is to protect the body from external substances and infectious agents. Barrier dysfunction could lead to the development of atopic dermatitis [8]. Epidermis also have a functional role for the induction of the cutaneous immune system to an external antigen. The induction of the cutaneous immune system is organized by langerhans cells [9], which reside in the epidermis. The induction is initiated when langerhans cells take up an external antigen [10], then langerhans cells detach from the epidermis to the dermis and present the captured antigen to T cells [9]. As these cells rarely exist in the epidermis, melanocytes are well known to produce melanin content, located in the basal layer of epidermis. Produced melanin in melanocytes are delivered to surrounding epidermal basal cells, followed by rearrangement of melanin above nuclei at the apical side in epidermal cells, known as supranuclear melanin cap. Melanin protects epidermal cells from damage caused by ultraviolet (UV) irradiations, as a natural UV protector. There are ethnic variations in melanin among races, resulting in

different physical appearances due to differences in the activity level of tyrosinase, a master enzyme that produces melanin [11, 12].

Dermis is mainly composed of dermal fibroblasts and connective tissue, formed by two different layers, papillary dermis adjacent to the epidermis and reticular dermis adjacent to subcutaneous tissue (Fig. 1-1). Papillary fibroblasts in papillary dermis, and reticular fibroblasts produce different compositions of extracellular matrix, reflecting on different physical properties between papillary and reticular dermis [13-17]. Dermal fibroblasts and mesenchymal cells in connective tissue, produce and secrete major extracellular matrix, various type of collagen, and components of elastic fibers, which is followed by the formation of collagen fibers and elastic fibers in the extracellular area. The major dermal extracellular matrix is collagen fibers which are extremely tough, providing mechanical strength to dermis and skin. The amount of connective tissue growth factor (CTGF), which regulates the production of collagen, decreases with aging, and may mechanically weaken the dermis of aged skin [18] . Elastic fibers are well known to play a crucial role in the elasticity of skin dermis and are also decreased with aging [19]. These decrease of elastic fibers in aged skin could lead to changes in appearance, such as skin sagging [20].

The skin, dermis and subcutaneous tissue is supported by a blood and lymph vascular

system [21, 22]. Like other organs, the blood vasculature in skin supplies nutrients and oxygen to surrounding cells and coordinates the immune system through leukocyte trafficking, including T cells and monocytes/macrophages. Lymphatic vasculature generally accompanies blood vasculature in dermis and subcutaneous tissue where it returns the extravasated fluid and macromolecules to the blood stream, which is a crucial event to maintain fluid balance in tissue [22]. Lymphatic vasculature also directs antigen-representing cells to the lymph node, modulating the immune system.

The subcutaneous tissue layer is underneath the dermis and composed mainly of adipose tissue and septa of connective tissue [23] (Fig. 1-1). Adipose tissue is formed mostly by mature adipocytes with lipid droplets. Adipocytes aggregate to form as fat lobules, and subcutaneous fat lobules are surrounded by fibrous septa of connective tissue. Since subcutaneous fat is mechanically flabby, due to its lipid composition, fibrous septa have a function to stabilize subcutaneous tissue through compartmentalization [23].

Skin appendages include hair follicles (Fig. 1-1, 1-2), sebaceous glands, sweat glands and arrector muscle pili, which each show their own characteristic physical features. These appendages are observed in skin at various frequencies, depending on the site of skin. For instance, the number of eccrine sweat glands show regional variation across the skin [24]. Hair follicles are at high density in scalp skin and at lower density at

other skin sites [25] and hand, foreskin, lip and palmoplantar skin include no hair follicles at all. The variety in the frequency of skin appendages affords different skin sites characteristic appearances.

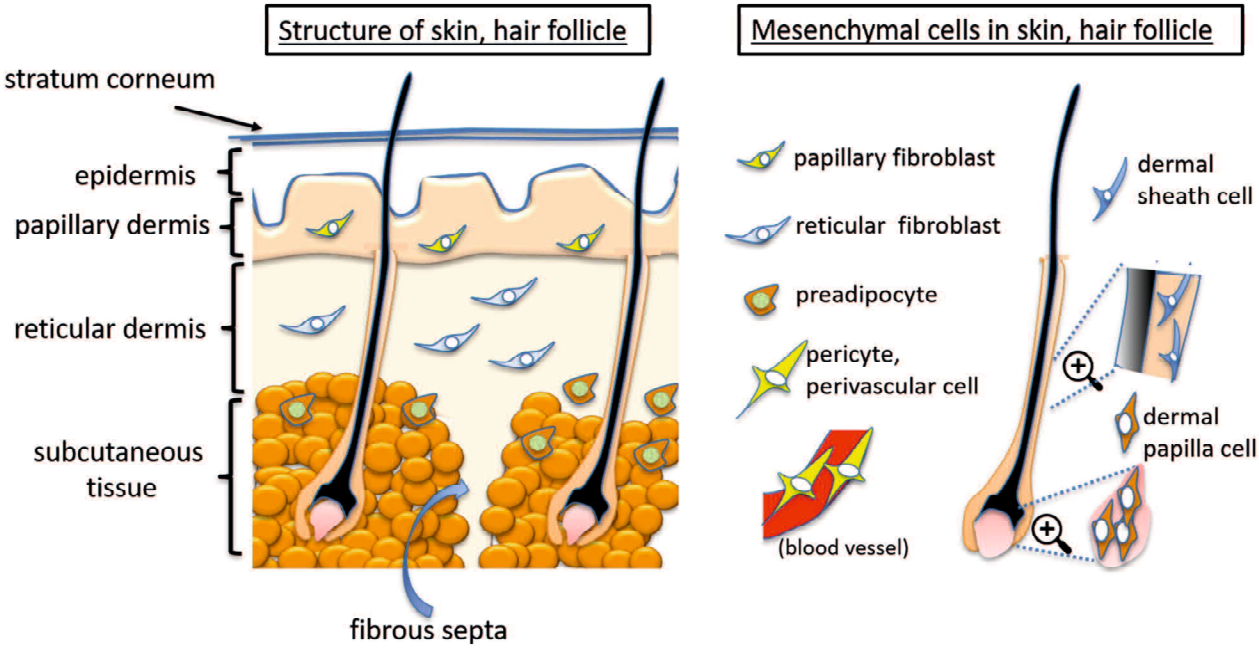

Figure 1-1. Structure of human skin, mesenchymal cells in skin and hair follicles

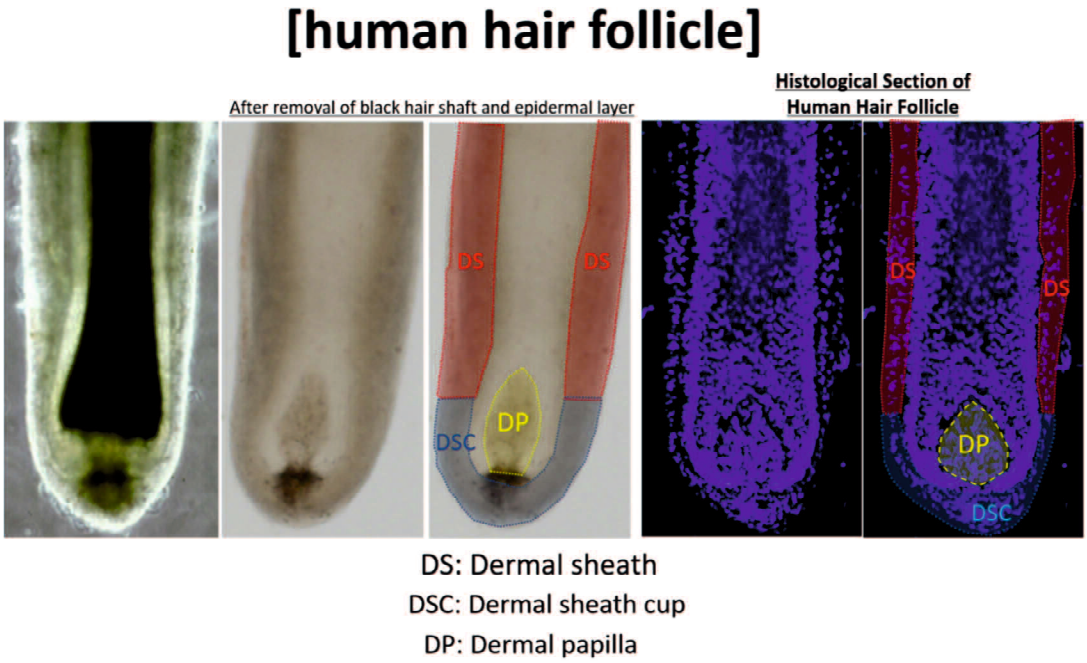

Figure 1-2. Histological structure of the human hair follicle

I.3 Skin diseases and characteristic skin appearances as clinical symptoms

In this chapter, clinical cases of skin disease will be introduced with their representative clinical symptoms. The lesions appearing on the skin are collectively called eruptions, or rashes, and eruptions with characteristic clinical appearances are given special names. They include erythema, which is observed when the blood vessels are congested under the epidermis, and purpura caused by intradermal bleeding due to trauma. Erythema might be clinical appearance of contact dermatitis that is caused by interaction with allergic substances such as infectious agents and specific drugs. If white or silvery scales are additionally observed, these clinical symptoms indicate psoriasis, which is a chronic inflammatory skin disease. Pigmentation disorders are collectively referred to as dyschromia. They include pigmented macule, which involves the deposition of melanin. Another form of dyschromia is vitiligo vulgaris in which melanocytes are gradually lost. These examples relate to the color of the skin surface, but there are also skin diseases that show extruded changes, such as papules, nodules and tumors that can be caused by dermatitis, dermal edema, and granulomatous disease. A disease associated with skin appendages that causes significant changes in appearance is androgenic alopecia, which causes hair thinning due to miniaturized hair follicles. In the descriptions above, the characteristic symptoms of the skin disease are restricted to the skin. However, there are

also clinical cases of systematic disorders where one end of a systematic change appears in the skin. For example, jaundice informs a decrease in liver function, and rapid pigmentation may be a skin symptom of serious disease, such as malignant melanoma that has metastasized to the whole body. Therefore, clarification of the mechanisms that cause changes in the appearance of the skin is important not only for the development of fundamental countermeasures against skin disease, but also for understanding change and effect in the whole body.

I.4 The role of mesenchymal cells in skin

The mesenchymal cells observed in skin include dermal fibroblasts, preadipocytes, pericytes (including perivascular cells) and specialized mesenchymal cells in human hair follicles (Fig. 1-1). The major role of mesenchymal cells in connective tissue is considered to be the production of extracellular matrix for the structural support of tissue, such as collagen and elastic fibers, As described above, dermal fibroblasts are classified into papillary fibroblasts and reticulated fibroblasts, each having different properties that are crucial to produce different connective tissues, such as papillary and reticular dermis [13-17]. Preadipocytes are precursor cells of mature adipocytes with lipid droplet existing in the lower part of the reticular dermis and adipose tissue, and are considered to be

involved in the formation of adipose tissue through differentiation into mature adipocytes. Perivascular pericytes cells are observed around blood vessels that are considered to have multi-differentiation potential like mesenchymal stem cells [26, 27] as they have been shown to promote epidermal regeneration in reconstituted human skin models [27]. At wounds sites myofibroblasts, derived from surrounding mesenchymal cells, promote wound healing through the secretion of growth factors and the production of extracellular matrix [28].

Mesenchymal cells are also observed in hair follicles (Fig. 1-1, 1-2), such as dermal papilla cells and dermal sheath cells. The dermal papilla is located at the bottom of the hair follicles, which play a crucial role in morphogenesis of hair follicles and also hair cycling [29]. It is also well known that the hair dermal papilla could form reconstituted hair follicles, showed by several rodent experimental assay [30]. Successful generation of reconstituted human hair follicles, using human dermal papilla cells, is a challenging task due, in part, to the loss of intrinsic potential of hair induction with cell culturing. Dermal sheath cells are located in connective tissue of the outermost layer of hair follicles. The dermal sheath is also known to have hair follicle regeneration ability but its characteristic properties are comparatively unclear compared with dermal papilla. In recent studies, skin mesenchymal cells were shown to differentiate from each common

ancestral cell located in the upper and lower layers of the developing dermis, and then these differentiated mesenchymal cells formed characteristic skin dermis layers [31]. Moreover, in adults some differentiated mesenchymal skin cells have multi-differentiation potential, such as perivascular cells, as described above. Other mesenchymal cells, such as dermal papilla cells also have multi-differentiation potential and show heterogeneity of cell population [32]. Some dermal sheath cells could also differentiate into other types of mesenchymal cells as skin-derived precursor cells [33]. Furthermore, at the bulge area of hair follicles, epidermal lineage-derived stem cells could differentiate toward to several types of mesenchymal cells [34]. Some preadipocytes play a crucial role in hair follicle regeneration by providing a niche to drive stem cell activation in the hair follicle [35]. From the background described above, some populations in differentiated mesenchymal cells could differentiate toward other types of mesenchymal cells, or lead stem cell activation through provision of niches, even in homeostatic conditions. These heterogeneous multi-differentiational events indicate heterogeneity of skin mesenchymal cell populations, and several studies reveal heterogeneity of dermal mesenchymal cells based on the specific expression of surface antigen. Hence, it is considered that the definition of the characteristic properties of each mesenchymal cell is important to understand the homeostatic state.

I.5 Experimental approaches and animal models in dermatological research

In dermatological studies, several experimental approaches of molecular biology have been applied, such as histological staining including immunohistochemistry, quantitative RT-PCT and ELISA assay for quantification of specific gene expression, gene microarray analysis for global expression profiling and various skin cell culture assays. Many *in vivo* rodent studies that target the loss or gain of gene function, such as knockout mouse models and transgenic mice, reveal a functional role of specific factors in skin development, maintenance of skin homeostasis and skin disease. Through these *in vivo* studies, several skin disease related animal models have been reported. Several psoriasis animal models, that mimic human psoriatic skin, have been reported and reviewed [36]. An atopic dermatitis mouse model [37] and an androgenic alopecia model mouse [38], which represents miniaturization of hair follicle with aging, have also been reported. Studies using these mice models could reveal the unknown mechanisms leading to skin diseases, and these mouse models could also be used for development of skin disease treatments. However, the differences between human and mouse skin should always be considered in dermatological studies. For instance, the epidermis and dermis are generally thicker in humans compared with mice. And densities of hair follicles are different between mouse back skin and human scalp skin, and the sizes of hair follicles are

obviously different. Periods of each hair stages in hair cycling are also different reflecting longer human hair length compared with shorter mouse coat hair. The immune system in the mice varies compared with that of humans in having different properties of inflammatory cells. In addition, the outbred human population could make it more complicated to understand mechanisms underlying human disease or any physiological phenomenon in humans. Taking into consideration these structural and physiological differences, many findings based on mouse experiments could still be useful to better understand the physiological phenomenon and physiology of human skin disease and to efficiently develop treatments.

I.6 Thesis objectives

As described above, clinical symptoms of appearance are crucial for clinical diagnosis of skin diseases. Many studies have been undertaken to understand the mechanisms that cause characteristic changes in skin appearance, not only for the development of medical treatment against disease, but also for consideration of its potential effect to the whole body systemically. In addition, recent findings have revealed that mesenchymal cells of the skin play various roles in skin physiology. The studies conducted in this thesis will investigate the mechanisms underlying characteristic changes

in skin appearance related to the hair follicle in CHAPTER II, and cellulite in CHAPTER III, with a focus on the modified mesenchymal cells.

In CHAPTER II, studies to understand the role of several types of hair dermal mesenchymal cells in hair cycling, morphogenesis and regeneration have been conducted. An androgenic alopecia, described briefly in CHAPTER I.3, significantly changes hair appearance as the miniaturized hair follicles result in noticeably thinner hair. Although it is understood that the mesenchymal cells, constituting the hair bulb located in the deepest part of the hair follicle, might be the causative mechanism to androgenic alopecia, there are still many unrevealed pathways. This thesis will investigate how various types of mesenchymal cells are involved in hair cycling, morphogenesis and regeneration and will discuss how they relate with hair disease, such as androgenic alopecia.

In CHAPTER III, the thesis will focus on cellulite, which is a skin condition characterized mainly by skin surface irregularities observed on the buttocks and thighs in the adult female. The mechanism that causes its appearance is unclear. Initial studies will identify the histological characteristics of cellulite skin tissue, and then research will be conducted to identify the physiological pathways underlying cellulite formation.

CHAPTER II:
Functional role of hair mesenchymal cells in hair follicle formation and cycling

II-1: Functional role of dermal sheath cells in hair cycling

II-1. 1 Background and objective

Dermal papilla (DP) and dermal sheath (DS) surround the periphery of hair follicles; both differ from epithelial cells, which comprise the majority of hair follicles, in that DP and DS are composed of mesenchymal-derived cell populations. DP cells are well-known to play crucial roles in mammalian hair follicle induction and cycling [30]. DS is located at the outer most border of the hair follicle and comprises the connective tissue sheath of follicles; DS cells are known to contribute to hair cycling and follicle neogenesis. At rat hair bulbs from which the rat vibrissa follicle has been removed, transplanted DS has been shown to regenerate DP and hair follicle tissue [39]. Peribulbar DS cells located at the bulbar part of the vibrissa DS can induce hair follicle development in the mouse [40]; DS in the upper part of rat vibrissa also has demonstrated the potential for hair regeneration [41]. Additional studies showed that human hair follicles can be regenerated from transplanted human DS; notably, DP originates from DS [42]. The above transplantation studies demonstrate that DS tissue and its derived cells can regenerate hair follicles in mammalian hair. Regarding the function of DS at steady state, DS cell proliferation in mice begins at early anagen; this is followed by proliferation of DP cells, indicating that some DP cells may originate in/migrate from DS cells [43]. In addition, progenitor cells (hair follicle dermal stem cells) in DS have been reported to produce DS

and DP cells during hair cycling [44]. These previous reports showed that DS cells are critical for hair cycling due to their regenerative potential; however, the characteristics of DS cells are not well-known, as described in CHAPTER I.4, particularly with respect to the underlying mechanism associated with hair cycling and regeneration. The aim of the present study was to investigate the characteristics of DS cells and the underlying mechanism by which they modulate hair cycling. In the present study, the transcriptional profile of human DS cells was analyzed, compared with the profiles of human DP cells and dermal fibroblasts (DFs) in early *in vitro* culture.

Among highly expressed genes in DS cells, we focused on CD36 and hepatocyte growth factor (HGF), because HGF affects hair growth and hair cycling [45], and is a well-known angiogenic factor [46]. In addition, CD36 is expressed in adipocytes, macrophages, and smooth muscle cells and capillary endothelial cells; CD36 is a receptor for thrombospondin-1, fatty acids, and collagen [47]. However, the function of CD36-expressing DS cells in human hair follicles is unclear. In the present study, the expression pattern of CD36 in DS cells and its potential functions in human hair follicles were investigated.

II-1. 2 Material and methods

Preparation of human primary cells

Human scalp tissues were obtained from patients undergoing plastic surgery, with the approval of the Ethical Committee of Shiseido Research Center. Our study was conducted in accordance with the tenets of the Declaration of Helsinki. Written informed consent was obtained from all participants. Human DP cells, DS cells, and DFs were expanded using explant culture with Dulbecco's Modified Eagle's Medium (Life Technologies, Carlsbad, CA) supplemented with 10% fetal bovine serum (FBS), 10 ng/mL epidermal growth factor, and 2 ng/mL basic fibroblast growth factor; they were then passaged *in vitro*. Human microvascular endothelial cells (HMVECs) were purchased from Toyobo (Osaka, Japan). HMVECs were grown in endothelial cell growth medium 2 (Lonza, Basel, Switzerland)

Microarray analysis

For gene microarray analyses, we prepared four lots of tissue-derived P2–P4 passaged DS cells, DP cells, and DFs isolated from two men (two lots of tissues from a 25-year-old man and two lots of tissues isolated from a 29-year-old man for explant culture). In this study, one lot of passaged cells was defined as those cells isolated from

the same piece of tissue for explant culture. Microarray analysis were performed to compare DP cells, DS cells, and DFs derived from the same pieces of tissue. Two-color oligo microarray analyses were performed to measure the fold change in a pair of Cyanine3 (Cy3)- and Cyanine5 (Cy5)-labelled samples; three pairs were compared with determine expression profiles of these three types of cells, as listed in Table 2-1. Indicated cyanine 3- and cyanine 5-labelled sample pairs were analyzed by two-color gene microarrays to compare the three different types of cells.

RNA was extracted using the Qiagen RNeasy Mini Extraction kit (Qiagen, Hilden, Germany), in accordance with the manufacturer's protocol. Double-stranded cDNA was synthesized from the total RNA, and then Cy3- or Cy5- labeled cRNA was made from the cDNA by *in vitro* transcription, using the Low RNA Fluorescent Linear Amplification kit, in accordance with the manufacturer's instructions (Agilent Technologies, Santa Clara, CA). Sample pairs were hybridized to two-color oligo microarray chips (Whole human Genome (44K), G4110F, Agilent Technologies), described in Table 2-1. The chips were washed as instructed by the manufacturer, and hybridized cRNA fluorescence on each chip was quantified in a microarray scanner (Agilent dual-laser Microarray scanner G2565AA). Scanned data were analyzed using Feature Extraction Software 9.1 (Agilent Technologies). For bioinformatics analysis, data were processed with Gene Spring GX

7.3.1 software, in accordance with the manufacturer's instructions (Agilent Technologies). After excluding genes that were absent in three of the four lots of sample pairs of DS/DP and DF/DS, those that were two-fold or higher in three of four samples (DS/DF and DS/DP) were selected (141 genes). The statistical significance of the enrichment of Gene Ontology categories (http://www.geneontology.org/) in the 141 selected genes was determined by Fisher's exact test.

Table 2-1.

Indicated cyanine 3- and cyanine 5-labelled sample pairs were analyzed by two-color gene microarrays to compare the three different types of cells.

	lots	Cy3	Cy5
Cy3-Cy5 pair	25M-1	DS (25M-1)	DP (25M-1)
		DP (25M-1)	DF (25M-1)
		DF (25M-1)	DS (25M-1)
	25M-2	DP (25M-2)	DS (25M-2)
		DF (25M-2)	DP (25M-2)
		DS (25M-2)	DF (25M-2)
	29M-1	DS (29M-1)	DP (29M-1)
		DP (29M-1)	DF (29M-1)
		DF (29M-1)	DS (29M-1)
	29M-2	DP (29M-2)	DS (29M-2)
		DF (29M-2)	DP (29M-2)
		DS (29M-2)	DF (29M-2)

Immunostaining

Human scalp tissues or dissected hair follicles were embedded in optimal cutting temperature compound (Sakura, Tokyo, Japan) and were sectioned at 7 μm thickness. After sections were fixed in 4% paraformaldehyde for 5 min, they were subjected to immunohistological staining as described in previous studies [48]. CD31(AF806), CD36(clone: FA6-152), and platelet-derived growth factor receptor (PDGFR)-β antibody (PA5-28527) were purchased from R&D systems (Minneapolis, MN), Biolegend (San Diego, CA), and Thermo Fisher Scientific (Waltham, MA). Signals were detected by commonly used Alexa 488- and Alexa 594-conjugated antibodies (Invitrogen, Carlsbad, CA), as appropriate.

Stages of the hair cycle in human hair follicles were classified using criteria reported in previous studies [49]. For immunocytochemistry of DS cells, CD36-expressing DS cells were detected with CD36 antibody. For whole-mount imaging of CD31 and CD36 expression in immunostained hair follicles, isolated hair follicles were fixed in 4% paraformaldehyde for 2 h at 4°C, followed by graded ethanol dehydration and rehydration. Follicles were treated with 5% Triton X-100 in phosphate-buffered saline (PBS) for 10 min, and then immunostained with CD31 and CD36 primary antibodies and corresponding Alexa fluorescent molecule-conjugated secondary antibodies (Invitrogen);

follicles were washed 6–8 times with 0.1% Tween-20 in PBS for 5 min per wash. DSs for whole-mount staining were dissected from hair follicles and were opened with scissors, followed by whole-mount staining as described above.

Quantitative real-time reverse transcription-polymerase chain reaction (qRT-PCR)

RNA was extracted with a Qiagen RNeasy Mini Extraction kit (Qiagen), in accordance with the manufacturer's protocol. cDNA was synthesized using a Superscript III kit with oligo dT primer (Invitrogen), in accordance with the manufacturer's protocol. Expression levels of human CD36 and HGF were investigated using FastStart SYBR Green Master Mix (Roche, Basel, Switzerland) and amplification was performed on a LightCycler 2.0 (Roche). Quantification of expression was performed using the $2^{-\Delta\Delta CT}$ method [50]. Relative expression levels were calculated using glyceraldehyde 3-phosphate dehydrogenase (*GAPDH*) as a reference gene. Primer pairs were designed as follows: *GAPDH* (5′-GCACCGTCAAGGCTGAGAAC-3′,

5′-ATGGTGGTGAAGACGCCAGT-3′);

CD36 (5′-GAGGAACTATATTGTGCCTATTCTTTGGC-3′,

5′-CATAAAAGCAACAAACATCACCACACCAAC-3′);

and *HGF* (5′-GAGGGAAGGTGACTCTGAATGAG-3′,

5′-AATACCAGGACGATTTGGAATGGCAC -3′).

The primer pairs were verified by melting curve analyses with single amplicons.

Co-culturing of CD36-enriched DS cells with HMVECs

CD36-enriched DS cells were prepared from DS cells by using CD36 antibody and MACS bead-conjugated antibodies (Miltenyi Biotech, San Diego, CA), in accordance with the manufacturer's protocol. Cells collected from column flowthrough were regarded as CD36-negative cells. CD36-enriched or -negative DS cells (1×10^5) were seeded in the above-described medium for explant cultures; on the next day, HMVECs (1×10^5) were additionally seeded in endothelial cell growth medium 2. Eight hours after co-culture was initiated, culture medium was replaced with 0.1% FBS in endothelial cell basal medium 2 (Lonza). Two days after replacing the medium, co-cultured cells were collected and the total numbers of cells were measured by Coulter counter Z-1 (Beckman Coulter, Fullerton, CA); subsequently, the proportions of CD31-positive cells in co-cultured cells were measured with flow cytometry (Guava EasyCyte, Millipore, Billerica, MA), in accordance with the manufacturer's protocol after tuning the setting for CD31-positive cells with reference to HMVECs. Immunocytochemistry for cytometry analyses was performed with fluorescein isothiocyanate-conjugated CD31 antibody (Abcam,

Cambridge, UK), in accordance with the method described by the manufacturer. The total number of cells was multiplied by the measured proportion of CD31-positive cells to calculate the number of putative CD31-positive HMVECs.

II-1. 3 Results

Gene expression profiling to characterize DS cells compared with DP cells and DFs

Gene microarray analysis demonstrated differential expression profiling among DP cells, DS cells, and DFs isolated from the same donor. DP and DS cells were prepared from hair follicles after excluding the hair shaft and epithelial sheath (Fig. 2-1-1c). Isolation of DS cells, DP cells, and DFs (Fig. 2-1-1d) was followed by gene microarray analysis after 2–4 passages. Isolated DS cells and DFs showed typical spindle bipolar shapes, whereas isolated DP cells showed comparatively rounded shapes (Fig. 2-1-1d). Two-color (Cy3 and Cy5) microarray analyses were employed to compare the three samples by inputting the fold changes of gene expression between DFs and DS cells, DS cells and DP cells, and DP cells and DFs. Line graphs of $\log_2$ fold change data were used to visualize the gene expression profiles of each sample included in each comparison (Fig. 2-1-1e–g). Visualization clearly showed that gene expression profiles of DFs differed from those of DS cells and DP cells (Fig. 2-1-1e, f). In addition, expression profiles of DS cells and DP cells were comparatively similar (Fig. 2-1-1g). Two lots of cells isolated from one donor were compared with two lots of cells isolated from another donor. Differential expression profiles were observed between cells from different donors (shown in Fig. 2-1-1e [DS/DP] and Fig. 2-1-1f [DF/DS]). However, there were minimal

differences in expression profiles between lots (tissue samples) from the same donor (Fig. 2-1-1e–g). One hundred forty-one genes were expressed two-fold or higher in DS cells, compared with DP cells and DFs. Gene ontology analysis of 141 genes highly expressed in DS cells indicated associations with angiogenesis and the vascular endothelial growth factor A signaling pathway, which has a crucial role in angiogenesis and modulation of blood vessels [51] (Fig. 2-1-1h).

Characteristics of capillary blood vessel networks in hair follicle DS during hair cycling

As gene expression profiling of DS cells indicated an association between DS cells and blood vessels, characteristics of blood vessels in DS were investigated by histological staining with an antibody against the vascular endothelial cell-specific marker, CD31. Histological studies showed blood capillaries in anagen follicles within DS and DP (Fig. 2-1-2a). Whole-mount staining showed characteristics of blood capillaries in hair follicle DS at anagen (Fig. 2-1-2c), catagen (Fig. 2-1-2e), and telogen (Fig. 2-1-2g). In anagen hair follicles, more dense capillary networks were observed immediately above the bulb region in DS, compared with other DS regions (Fig. 2-1-2c, arrows). Furthermore, broken capillary networks were observed in catagen hair (Fig. 2-1-2e, arrowheads), whereas sparse capillary networks were observed in telogen hair (Fig. 2-1-2g). These results

implied that capillary networks in DS are formed by angiogenesis during human hair cycling, which is consistent with a previous report in mice [52, 53].

CD36 and HGF are highly expressed in DS cells, and localization of CD36-expressing DS cells is associated with blood capillary formation

Blood capillary networks change dramatically during hair cycling; thus, to investigate the characterization of DS cells associated with hair cycling through blood capillaries, we focused on CD36 and HGF, which were highly expressed in DS, as demonstrated by present gene array analyses; these proteins are known to have functional roles associated with blood vessels [46, 47]. To precisely measure differential expression of CD36 and HGF between DS cells and DP cells, qRT-PCR analyses were performed with five pairs of DS cells and DP cells from the same donors. Expression levels of CD36 and HGF in DS cells were significantly higher than those in DP cells, regardless of donor differences (Fig. 2-1-3a). qRT-PCR analyses with pooled samples (DS cells from five donors compared with DP cells from five donors) indicated that CD36 and HGF were significantly more highly expressed in DS cells than in DP cells (Fig. 2-1-3b).

CD36 immunostaining of DS cells revealed CD36 expression in DS cells; however, CD36-expressing cells were not observed in DP cells or DFs (Fig. 2-1-3c), consistent with microarray and qRT-PCR analyses. Immunohistochemistry revealed expression of

CD36 in hair follicles at anagen V–VI (Fig. 2-1-3d, e), regarded as mature hair follicles [49]. CD36 was expressed only in cells in the upper DS, not in the lower DS or DP (Fig. 2-1-3d); in addition, blood capillaries were consistently observed (Fig. 2-1-3d, lower image). Whole-mount staining showed that CD36-expressing cells were observed at the perivascular regions of capillary blood vessels (Fig. 2-1-3e); in particular, large numbers of CD36-expressing cells were present in a dense network of capillaries immediately above the bulb region (Fig. 2-1-3e). Blood capillaries were observed in hair follicles at anagen III (Fig. 2-1-3f) and anagen IV (Fig. 2-1-3g), which are regarded as premature anagen [49]. In this premature stage of hair follicle growth, CD36-expressing DS cells were observed at the perivascular region in the entire lower DS (Fig. 2-1-3f, g), whereas CD36-expressing DS cells were not observed in the lower DS in mature hair follicles at anagen V–VI (Fig. 2-1-3d). These histological studies suggested that CD36-expressing DS cells participated in blood capillary formation (i.e., angiogenesis), which might occur during maturation of hair follicles.

CD36-enriched DS cells promote proliferation of vascular endothelial cells

As our histological studies indicated that CD36-expressing DS cells may be associated with angiogenesis, particularly at premature hair follicles, we assessed whether

CD36-expressing cells affected angiogenesis. Angiogenesis progression is characterized by proliferation of endothelial cells as a key event [54]. Immunostaining results (Fig. 2-1-3c), which showed that CD36-expressing cells were a small population of DS cells, implied that enrichment of CD36-expressing cells could facilitate investigation of the association between CD36-expressing DS cells and angiogenesis. MACS bead sorting using a CD36 antibody showed successful enrichment of CD36-expressing DS cells from total DS cells. Gene Go ontology analyses of highly expressed genes in DS cells showed functional associations of DS cells with blood vessels. As whole-mount imaging showed abundant blood capillary networks in DS, we performed flow cytometry analyses of CD31-positive cells among DS cells (Fig. 2-1-4) to exclude the possibility that blood endothelial cells had been included, before focusing on the functional association of DS cells with blood vessels. Flow cytometry analyses of CD31 confirmed that blood endothelial cells were not included in DS cells, regardless of CD36 enrichment (Fig. 2-1-4). Sorted CD36-enriched DS cells were co-cultured with HMVECs (Fig. 2-1-5a) and compared with CD36-negative DS cells co-cultured with HMVECs (Fig. 2-1-5b). A higher number of CD31-expressing HMVECs was observed after co-culture with CD36-enriched DS cells, compared with HMVECs that had been co-cultured with CD36-negative DS cells. Measurement of the number of co-cultured HMVECs showed

increased numbers of HMVECs after co-culture with either CD36-enriched DS cells or co-culture with CD36-negative DS cells, compared with control (cultured HMVECs alone), due to the feeder effect (Fig. 2-1-5c). Co-culture with CD36-enriched DS cells resulted in a significant increase in the number of HMVECs, compared with the number of HMVECs after co-culture with CD36-negative DS cells (Fig. 2-1-5c). Exposure to conditioned medium from CD36-enriched DS cells did not increase proliferation of HMVECs, compared with CD36-negative DS cells (Fig. 2-1-6); thus, we concluded that CD36-enriched DS cells promoted proliferation of blood endothelial cells in a cell–cell contact-dependent manner. CD36-enriched DS cells showed increased HGF expression relative to that of CD36-negative DS cells, as measured by qRT-PCR (Fig. 2-1-5d); this indicated that CD36-expressing DS cells also expressed HGF, which is a known pro-angiogenic factor. These results suggested a possible mechanism for the proliferative effect of CD36-expressing DS cells on blood endothelial cells, associated with the expression of HGF.

II-1. 4 Discussions

In the present study, characteristics of DS cells were assessed by gene expression profiling and immunostaining to elucidate the expression patterns of specific genes in DS. Gene microarray analyses showed similar gene expression profiles between DS cells and DP cells, which differed from those of DFs (Fig. 2-1-1e–g). Similarities between DS cells and DP cells were described in some previous reports, as some DS cells constituted progenitor cells that differentiated into DP cells [43, 44].

Blood vessels in hair follicles in human scalp tissue were previously studied histologically [55, 56]. In those studies, Azo-dye staining was used to detect non-specific alkaline phosphatase in 30–75-μm-thick sections; this revealed capillary networks in hair follicles at anagen, catagen, and telogen. In the present study, to clearly observe capillaries in DS, a whole-mount immunostaining technique was used to detect hair follicles with a vascular endothelial cell-specific marker, CD31. A dense capillary network was present immediately above the bulb portion (Fig. 2-1-2c). Hair matrix cells, which envelope the DP at the hair bulb, rapidly proliferate to maintain hair growth in mature anagen hair follicles. Further studies are needed to understand the functional roles of these dense capillaries at the DS region immediately above the hair bulb. Our whole-mount imaging showed that regressed blood capillaries comprised broken capillaries with remaining

connective tissue at catagen hair follicles (Fig. 2-1-2e). This implied that blood capillaries in human hair follicles are remodeled during the hair cycle, consistent with a previous study in mice [52, 53]; thus, angiogenesis might occur during the transition from telogen to anagen phase in human hair follicles.

CD36 was highly expressed in DS cells, compared with DP cells and DFs (Fig. 2-1-3a, b). CD36-expressing cells were observed in the perivascular area in DS (Fig. 2-1-3e); however, CD36-expressing cells were not observed in the lower DS or the DP (Fig. 2-1-3d). To investigate possible involvement of blood capillary pericytes in hair follicles, immunostaining of a pericyte marker, PDGFR-β, was performed together with immunostaining of CD31 or CD36 (Fig. 2-1-7). PDGFR-β-expressing pericytes were observed at the perivascular area in DP and DS, whereas CD36-expressing cells were not observed in the lower DS or the DP. CD36 is reportedly expressed by adipocytes, macrophages, smooth muscle cells, and capillary endothelial cells [47]. In fact, cultured HMVECs showed minimal expression of CD36, compared with that in DS cells (Fig. 2-1-5a, b). It is unlikely that endothelial cells were included in the isolated DS cells; this was confirmed by flow cytometry analyses for CD31 (Fig. 2-1-4). Further histological staining is needed to confirm whether CD36-expressing cells could be perivascular macrophages or smooth muscle cells. As described in CHAPTER I.4, some of the

perivascular cells are considered to have multi-differentiation potential like that of mesenchymal stem cells [26, 27]. Some dermal sheath cells could also differentiate into other types of mesenchymal cells as skin-derived precursor cells [33]. These reports led to the idea of using CD36-expressing DS cells to show stem cell-like potential. Although further functional studies are needed to assess the stem cell-like properties of CD36-expressing, and CD36-expressing DS cells could be used as part of a cell-based therapy, likely mesenchymal stem cells.

In hair follicles at anagen III and IV (Fig. 2-1-3f, g), which are regarded as premature hair follicles, CD36-expressing DS cells were observed in the perivascular region in the lower DS, whereas CD36-expressing DS cells were not observed in mature hair follicles at anagen V–VI (Fig. 2-1-3d). Since an angiogenesis might occur during maturation of hair follicles, the association between CD36-expressing DS cells and angiogenesis was indicated. In fact, CD36-enriched DS cells promoted the proliferation of blood endothelial cells in a cell–cell contact-dependent manner (Fig. 2-1-5a–c). These results implied that CD36 participated in angiogenesis. Although the secreted factor, HGF (regarded as an angiogenic factor [46]) was expressed at higher levels in CD36-enriched DS cells (Fig. 2-1-5d), conditioned medium from CD36-enriched DS cells did not promote proliferation of HMVECs (Fig. 2-1-6). Thus, further studies are needed to

determine the mechanism by which CD36-expressing DS cells participate in angiogenesis.

Blood vessels dramatically change during murine hair cycling [52, 53]; angiogenic factors increase the hair growth and size of murine hair follicles [52], while inhibitors of angiogenesis regulate the hair cycle in an opposing manner [53]. These previous studies in mice revealed that blood vessel remodeling is associated with hair cycling and hair follicle size. Interestingly, CD36 is a receptor of thrombospondin-1, which reportedly reduces perifollicular angiogenesis and eventually delays hair growth [57]. HGF was highly expressed in DS cells, compared with DP cells (Fig. 2-1-3a, b); it was particularly highly expressed in CD36-enriched DS cells (Fig. 2-1-5d). HGF is known to affect hair growth and hair cycling [45], and is regarded as an angiogenic factor [46]. Although our present findings indicated that CD36-expressing DS cells may modulate blood capillary formation in human hair follicles, further studies are needed to determine the mechanism by which DS cells participate in human hair cycling and serve as progenitors of DP cells.

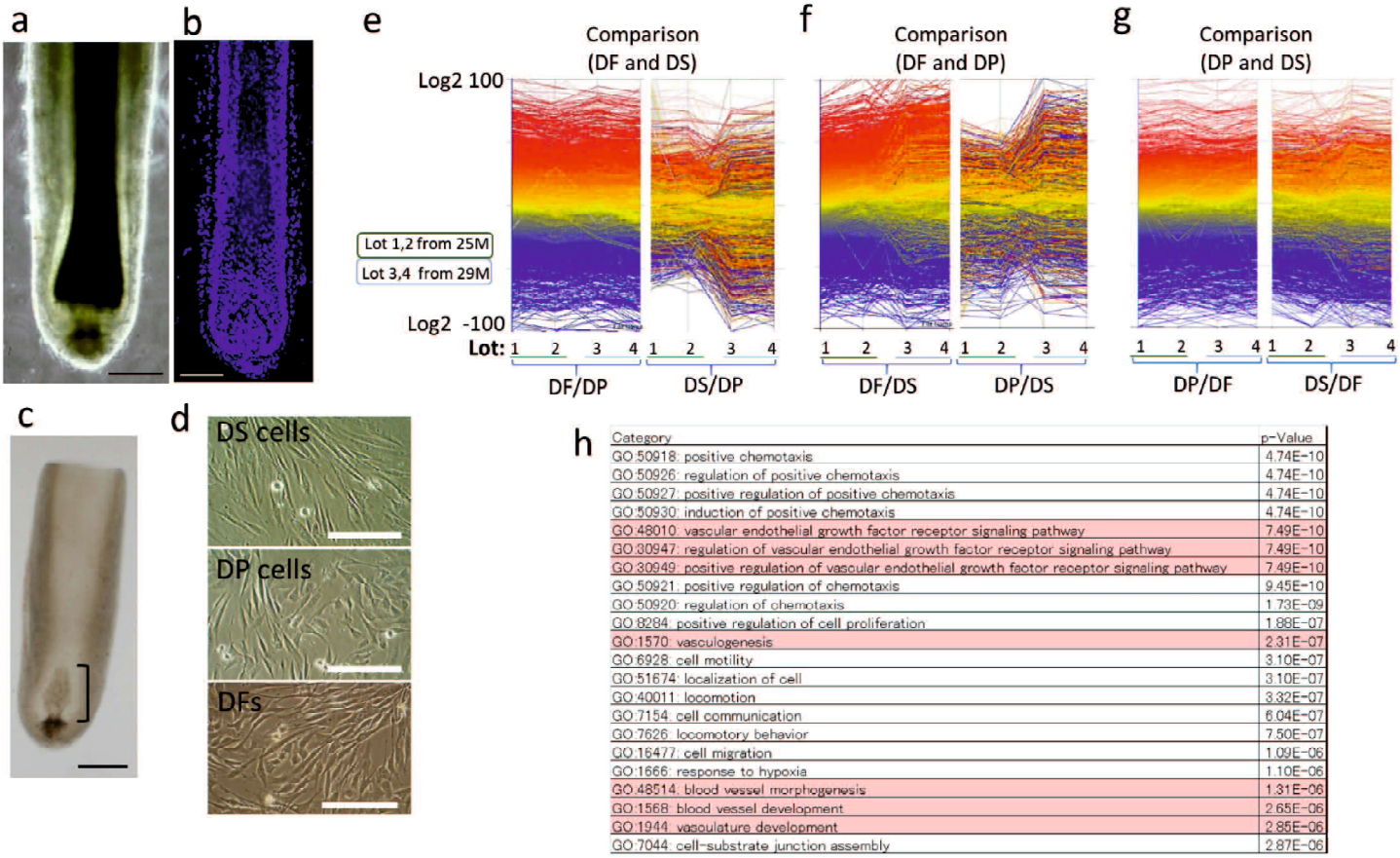

h

Category	p-Value
GO:50918: positive chemotaxis	4.74E-10
GO:50926: regulation of positive chemotaxis	4.74E-10
GO:50927: positive regulation of positive chemotaxis	4.74E-10
GO:50930: induction of positive chemotaxis	4.74E-10
GO:48010: vascular endothelial growth factor receptor signaling pathway	7.49E-10
GO:30947: regulation of vascular endothelial growth factor receptor signaling pathway	7.49E-10
GO:30949: positive regulation of vascular endothelial growth factor receptor signaling pathway	7.49E-10
GO:50921: positive regulation of chemotaxis	9.45E-10
GO:50920: regulation of chemotaxis	1.73E-09
GO:8284: positive regulation of cell proliferation	1.88E-07
GO:1570: vasculogenesis	2.31E-07
GO:6928: cell motility	3.10E-07
GO:51674: localization of cell	3.10E-07
GO:40011: locomotion	3.32E-07
GO:7154: cell communication	6.04E-07
GO:7626: locomotory behavior	7.50E-07
GO:16477: cell migration	1.09E-06
GO:1666: response to hypoxia	1.10E-06
GO:48514: blood vessel morphogenesis	1.31E-06
GO:1568: blood vessel development	2.65E-06
GO:1944: vasculature development	2.85E-06
GO:7044: cell-substrate junction assembly	2.87E-06

Figure 2-1-1. Gene expression profiling of dermal sheath (DS) cells reveals an association between DS cells and blood vessels

Images of (a) isolated hair follicle, (b) section of hair follicle, and (c) hair follicles after removal of epithelial portion (including the hair shaft). Bracket (c) indicates dermal papilla (DP). Isolated DS cells, DP cells and dermal fibroblasts (DFs) are shown (d). Line graphs of $\log_2$ fold change of DF/DP cells and DS cells/DP cells for comparison between DFs and DS cells (e); colors were assigned based on the first samples of DFs/DP cells. Number 1 and 2 cells were isolated from a 25-year-old man, whereas 3 and 4 were from a 29-year-old man. Line graphs of $\log_2$ fold changes of DFs/DS cells and DP cells/DS cells for comparison between DFs and DP cells (f); colors were assigned based on the first samples of DFs/DS cells. Line graphs of $\log_2$ fold change of DP cells/DFs and DS cells/DFs for comparison between DP cells and DS cells (g); colors were assigned based on the first samples of DP cells/DFs. (h) Category lists of gene ontology analyses with 141 genes highly expressed in DS cells compared with DP cells and DFs, shown with calculated p-values. Pink-highlighted columns show the categories associated with blood vessels. Bars = 200 µm (a–d).

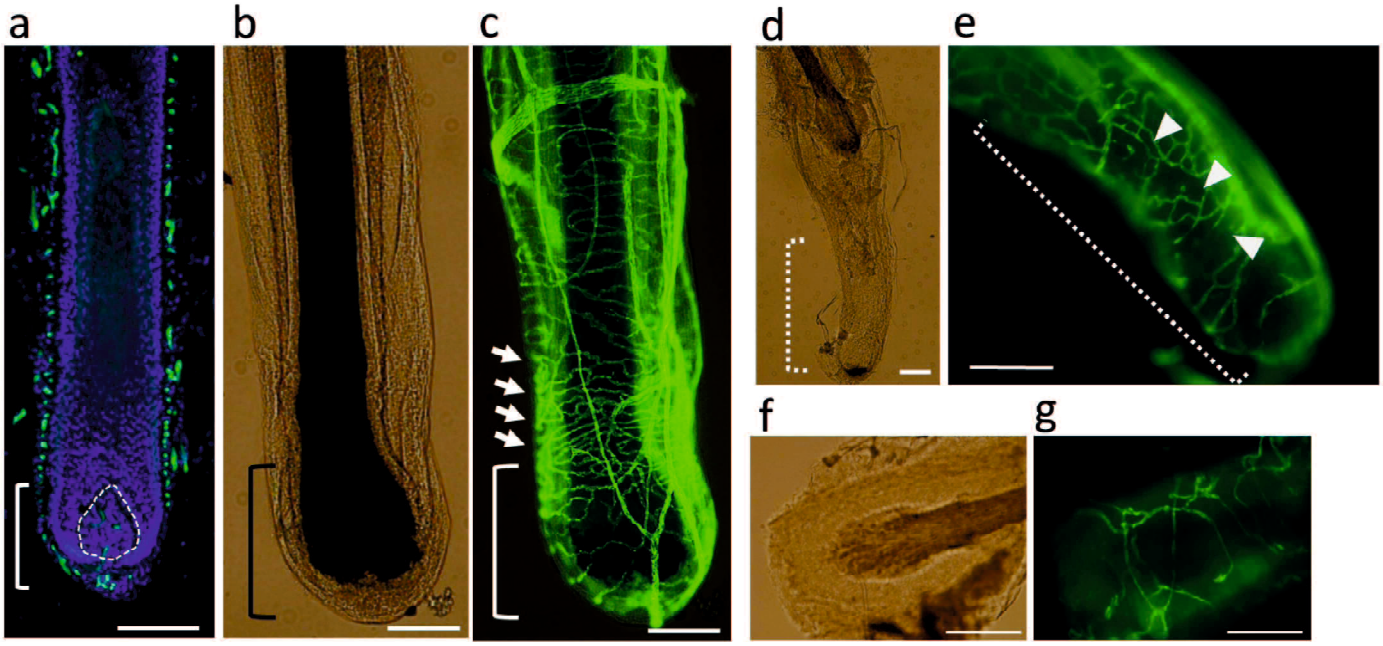

Figure 2-1-2. Blood capillaries in dermal sheath (DS) of hair follicle change with hair cycling, indicating new formation of capillaries during hair cycling

Immunohistochemical staining of endothelial cell marker CD31, detected by Alexa 488 green fluorescence. Blue indicates nuclei of cells stained with Hoechst 33342. Representative images of hair follicle sections immunostained for CD31 (a). Bright-field images of hair follicles at anagen for whole-mount staining (b). Whole-mount images of hair follicles at anagen immunostained for CD31, merged with bright-field images (c). Whole-mount images of hair follicles immunostained for CD31 at catagen (e) and telogen (g), merged with bright-field images at each stage (d and f). Brackets (a–c) indicate hair bulb regions of hair follicles. Closed area by dashed line (a) indicates dermal papilla (DP). Arrows (c) indicate dense networks of blood capillaries. Dashed line brackets (d, e) indicate region of regressed connective tissue at catagen. Arrowheads (e) indicate broken blood capillaries. Bars = 200 μm (a–g).

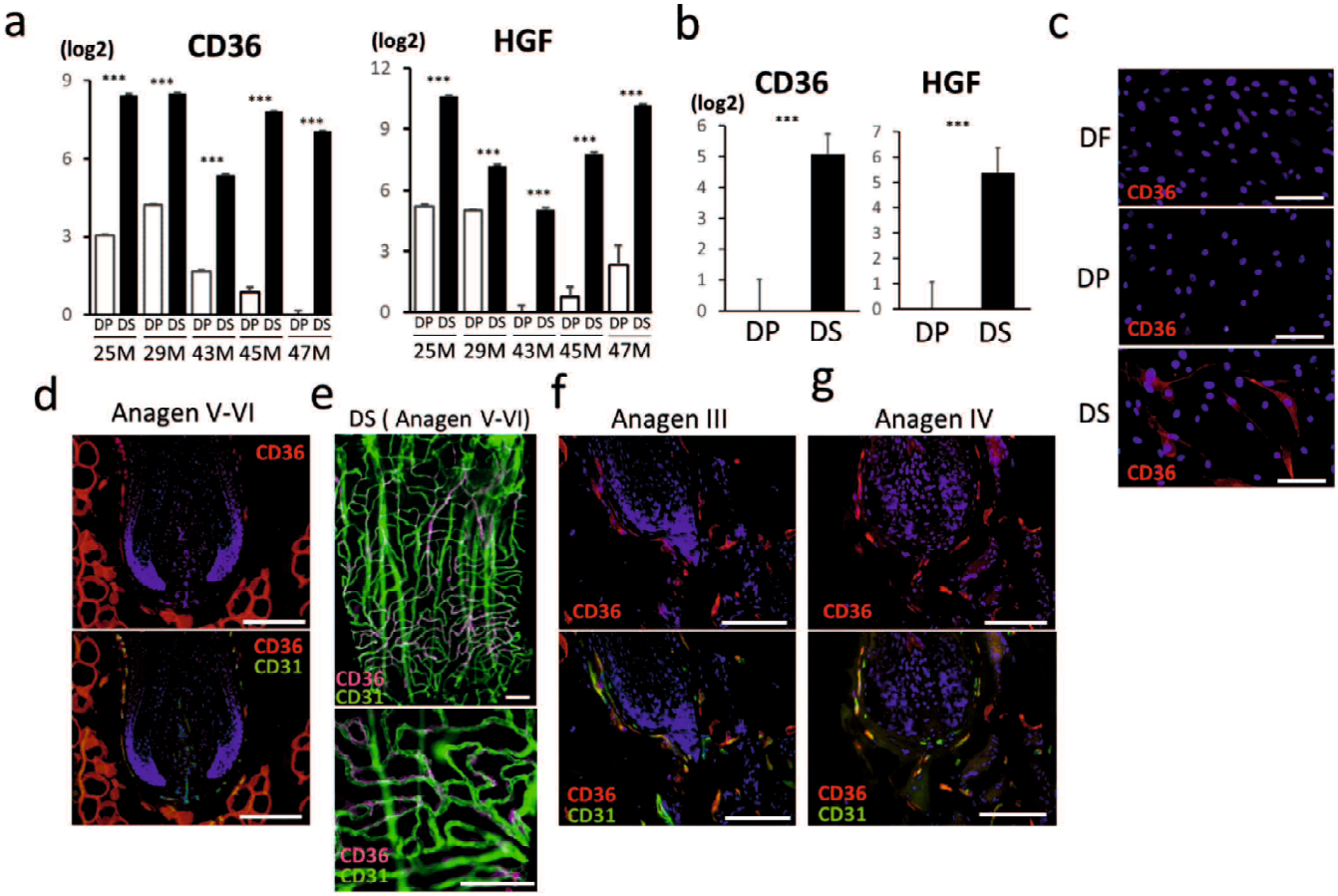

Figure 2-1-3. CD36 and hepatocyte growth factor (HGF) are highly expressed in dermal sheath (DS) cells, and CD36-expressing cells are observed in perivascular regions

(a, b) qRT-PCR analyses of CD36 and HGF. (a) Comparison of CD36 and HGF expression levels between DS cells and dermal papilla (DP) cells from same donor (n = 3): 25, 29, 43, 45, and 47-year-old men. Results are expressed as $\log_2$ fold change in donor-derived DS cells and DP cells over samples with smallest expression levels (DP cells from 47-year-old man for CD36, DP cells from 43-year-old man for HGF). (b) Comparison of expression levels of CD36 and HGF between collected samples of DS cells and DP cells. (n = 15) (b). Results are expressed as $\log_2$ fold change in collected DS cells over collected DP cells. Input was normalized to GAPDH; results are expressed as means ± S.D. Student's t-test was used for comparison between DS cells and DP cells. ***P < 0.001. Immunostaining of dermal fibroblasts (DFs), DP cells, and DS cells for CD36 (c) shows CD36 expression only in DS cells. Immunostaining for CD31 (green) and CD36 (red) in hair follicles at anagen V–VI (d), anagen III (f), and anagen IV (g). Whole-mount immunostaining for CD31 (green) and CD36 (purple) of dissected and "opened" DS at anagen V–VI (e). Blue indicates nuclei of cells stained with Hoechst 33342. Bars = 100 μm (c–g).

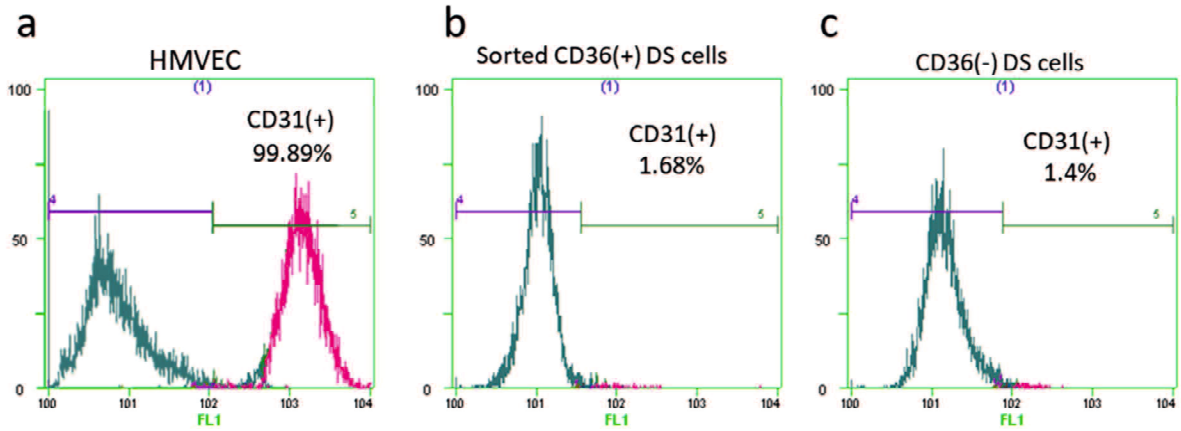

Figure 2-1-4. Flow cytometry analysis shows the proportion of CD31-positive vascular endothelial cells in sorted dermal sheath (DS) cells

CD31-positive endothelial cells are not included in sorted CD36-enriched (+) dermal sheath (DS) cells or in CD36-negative (-) DS cells. The proportions of CD31 (+) cells in HMVECs (a), CD36-enriched (+) DS cells (b) and CD36-negative (-) DS cells (c) were analyzed by flow cytometry. Numbers indicate the percentages of CD31-positive cells included in samples. Based on the fluorescence signal intensity of fluorescein isothiocyanate, fractioning settings were set. Blue bar indicates the negative fraction and red bar indicates the positive fraction commonly used in all analyses.

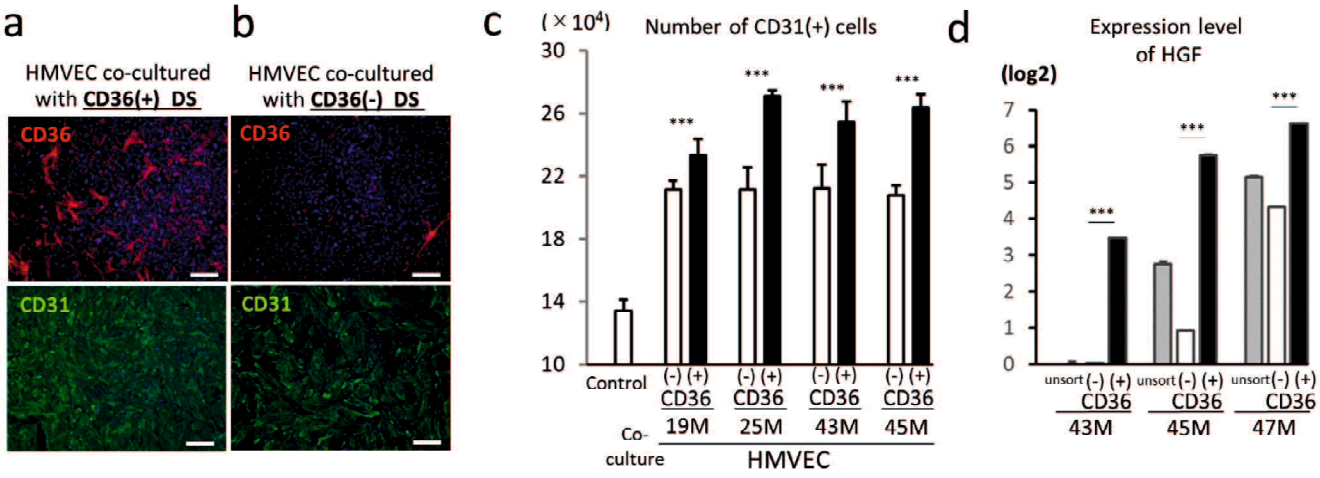

Figure 2-1-5. CD36-enriched dermal sheath (DS) cells promote proliferation of endothelial cells

Immunostaining for CD31 and CD36 in co-cultured CD36-enriched (+) DS cells and human microvascular endothelial cells (HMVECs) (a) and in co-cultured CD36-negative (-) DS cells and HMVECs (b). (c) Measurements of number of CD31-positive (+) endothelial cells in each co-cultured sample and control (0.1% FBS in endothelial basal medium 2) (n = 3). Results are expressed as means ± S.D. Student's t-test was used for comparison between HMVECs co-cultured with CD36-enriched (+) and CD36-negative (-) cells from same donor (n = 3): 19, 25, 43, and 45-year-old men, labeled as 19M, 25M, 43M, 45M. ***P < 0.001. (d) qRT-PCR analyses of HGF. Comparison of expression levels of HGF between CD36-enriched (+) and CD36-negative (-) DS cells from indicated donors and unsorted DS cells. Results are expressed as $\log_2$ fold change in each sample over unsorted DS cells from a 43-year-old man with negligible expression levels. Input was normalized to GAPDH; results are expressed as means ± S.D. Student's t-test was used for comparison between CD36-enriched (+) and CD36-negative (-) DS cells. ***P < 0.001. Bars = 100 μm (a–b).

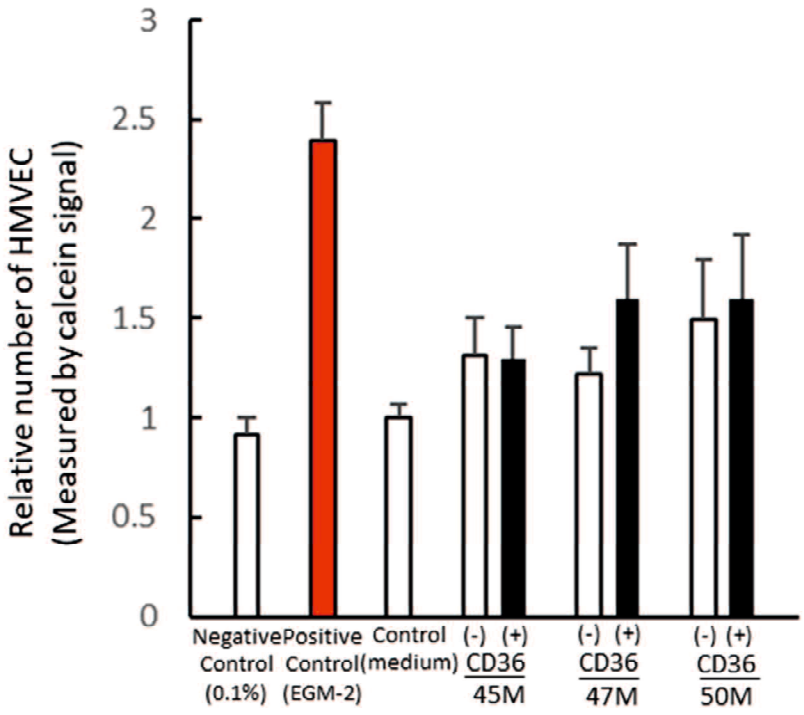

Figure 2-1-6. Assessment of the proliferative effect of conditioned medium

Assessment of proliferative effect of conditioned medium (24 h in 1% FBS supplemented DS medium), by sorted CD36-enriched (+) DS cells compared to CD36-negative (-) DS cells, negative control (0.1% FBS supplemented endothelial cell basal medium 2), positive control (endothelial cell growth medium 2), control (1% FBS supplemented DS medium). Relative number of HMVECs cultured in indicated medium were measured by Calcein-AM staining, followed by measuring intracellular incorporated Calcein fluorescent signal by fluorescent plate reader. There are no significant differences in the proliferative effect between conditioned medium of CD36-negative (-) DS cells and one of CD36-enriched (+) DS cells.

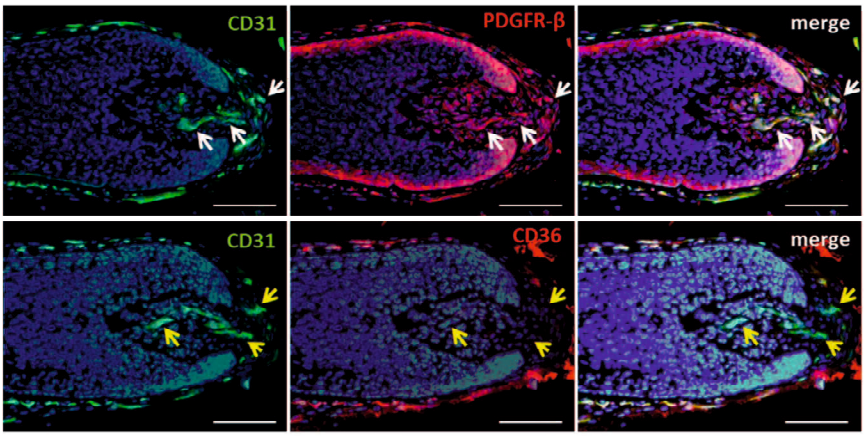

Figure 2-1-7. Localization of platelet-derived growth factor receptor (PDGFR)-β-expressing pericytes and CD36-expressing perivascular cells in dermal sheath (DS)

Immunostaining for endothelial cell marker CD31, pericyte marker PDGFR-β, and CD36. Representative images of hair follicle sections at bulb region immunostained with CD31 and PDGFR-β (upper images), and with CD31 and CD36 (lower images). White and yellow arrows in images indicate regions where capillaries are observed in the lower portion of dermal sheath and DP. White arrows indicate the same region in upper three images, yellow arrows indicate the same region in lower three images. PDGFR-β expressed pericytes are observed in DS and DP, however, CD36 expressed cells are not observed in lower DS and DP. Bars = 100 μm.

II-2: Generation of human reconstituted hair follicles in humanized skin using stimulated dermal papilla cells, and assessments of hair regenerative potential of dermal sheath cup cells

II-2. 1 Background and objective

Dermal papilla (DP) cells play crucial roles in mammalian hair follicle induction and cycling [30]. Although previous studies showed that human DP cells form hair follicle-like structures upon grafting[58, 59], generation of reconstituted skin composed by human cells with enriched hair follicles has not yet been accomplished. As DP cells are known to lose their ability for hair induction with passaging, several approaches have been attempted to maintain the hair-inducing ability of cultured DP cells [60, 61]. One such approach is activation of canonical Wnt signaling, whose importance in hair follicle formation is well documented [62]. For this purpose, the glycogen synthase kinase three beta inhibitor CHIR99021 can reportedly activate Wnt/β-catenin signaling without serious cell toxicities [63]. In addition to modulating signaling pathways, morphological approaches should be considered. A previous report suggested that three-dimensional (3D) spheroid-cultured human DP cells restored signature DP features [64]. However, despite several attempts to produce human hair follicles by stimulating DP cells, there is no report of successful reconstitution of whole skin and appendages (including hair follicles with cells of human origin) on the back skin of a host rodent species, such as mice. In the present study, we considered optimization of culture methods for DP cells to enhance their hair-inducing ability, such as activation of Wnt signaling and modified 3D

spheroid culture, as key elements for generating reconstituted human skin with functional hair follicles.

Although various methods for 3D spheroid culture are available, such as floating drop, U-bottom dish, and self-aggregation methods, the best method for stimulating DP cultures to maintain their hair-inducing ability is unknown. Moreover, whether the canonical Wnt signaling activator CHIR99021 can synergistically affect the hair-inducing ability of 3D spheroid-cultured DP cells is unknown.

In the present study, expression of several DP signature genes was assessed by qRT-PCR, such as LEF1, versican, BMP4, Sox2, and noggin which are thought to be associated with hair-inducing ability [60, 65, 66]. After optimization of the method for DP cell culture by measuring expression levels of these signature genes, we performed *in vivo* grafting experiments to assess hair-inducing ability. Among the different methods previously reported to assess hair inducing ability [30, 67], a "reconstituted human skin assay" [67] was employed as it is thought to be suitable for the purpose of *de novo* generation of reconstituted whole skin with enriched hair follicles. Finally, to evaluate the functional features of reconstituted human skin and hair follicles, injection of human dermal sheath cup (DSC) cells was performed. DSC cells are isolated from dermal sheath at peribulbar area in hair follicle, in other words, dermal sheath cup. Cultured mouse DSC

cells can contribute to dermal sheath and DP, as injected DSC cells reportedly incorporated into both DP and sheath areas of mouse hair follicles [40]. Thus, localization of injected human DSC cells in reconstituted skin was examined to reveal incorporation into the dermal sheath of hair follicles, which implies functional features of reconstituted human skin and hair follicles.

II-2. 2 Material and methods

Cell culture and cDNA library preparation

Human scalp tissues were obtained from a plastic surgeon with approval from the Ethics Committee of Shiseido Research Center. Our study was conducted in accordance with the Declaration of Helsinki. Human DP cells were expanded from explant cultures in Amniomax C100 complete medium or MesenPRO RS medium (Life Technologies, Carlsbad, CA). Seeded DP cells were maintained in a 37ºC incubator with 95% O_2 and 5% CO_2. For 3D-spheroid culture, 0.18–0.48 × 10^6 passaged DP cells were seeded on 35-mm EZ-sphere (Iwaki, Shizuoka, Japan), Elplasia MPc 500 (Kuraray, Osaka, Japan), or 35-mm NanoCulture MS pattern (SCIVAX LifeSciences, Kawasaki, Japan) dishes according to the manufacturers' protocols. At 72 h after seeding of DP cells, formed DP spheroids were collected. CHIR99021 was purchased from Axon Medchem (Groningen, Netherlands). For CHIR99021-stimulated DP cells, cells were cultured with medium containing CHIR99021 (3 μM) for 72 h. For CHIR99021-stimulated DP spheroids, CHIR99021-stimulated DP cells were seeded with medium containing 3 μM CHIR99021. For PKH labeling of DPCs, a PKH26 kit (Sigma-Aldrich, St. Louis, MO) was used according to the manufacturer's protocol. Seeded DPCs were maintained in a 37ºC incubator with 95% O_2 and 5% CO_2. RNA was extracted with a Qiagen RNeasy Mini

Extraction kit (Qiagen, Hilden, Germany) according to the manufacturer's protocol. cDNA was synthesized using a high capacity RNA-to-cDNA kit (Applied Biosystems, Carlsbad, CA) according to the manufacturer's protocol.

Quantitative real-time reverse transcription-polymerase chain reaction (qRT-PCR)

Expression of human LEF-1, versican, BMP4, noggin, and Sox2 was investigated using LightCycler 480 SYBR Green Master (Roche, Basel, Switzerland) and LightCycler 480 II (Roche) according to manufacturer's protocol. Quantification of expression was performed using the $2^{-\Delta\Delta CT}$ method [50]. Relative expression levels were calculated using glyceraldehyde 3-phosphate dehydrogenase (GAPDH) as a reference gene. Primer pairs were designed as follows: Sox2 (5′-GGAAATGGGAGGGGTGCAAAAGAGG-3′, 5′-TTGCGTGAGTGTGGATGGGATTGGTG-3′); and GAPDH (5′-GAGTCAACGGATTTGGTCGT-3′, 5′-TGGGATTTCCATTGATGACA-3′). Designed primer pairs were verified by analyzing the melting curve with single amplicons. Primer pairs for LEF1, versican, BMP4, and noggin were purchased as QuantiTech primers from Qiagen. For comparison between monolayer culture and each 3D-spheroid culture method, Dunnet's multiple test was applied using Kaleida Graph ver4.1 software (Synergy Software, Reading, PA). To assess the interaction between CHIR99021

stimulation and 3D-spheroid culture on expression, two-way ANOVA was performed using Kaleida Graph ver4.1 software.

Reconstituted human skin assay

To assess the contribution of DP spheroids to hair formation, we modified a previously reported "Reconstituted skin assay" [67]. Briefly, fetal human epidermal keratinocytes (HEK) and dermal fibroblasts (DFs) were purchased from ScienCell Research Laboratories (ScienCell, Carlsbad, CA). HEK were grown in EpiLife Basal Medium (Life Technologies) supplemented with EpiLife Defined Growth Supplement (Life Technologies) on flasks coated with iMatrix (Nippi, Tokyo, Japan). DFs were grown in DMEM/F12 (3:1) containing 1% antibiotic/antimycotic (100×) (Nacalai Tesque, Kyoto, Japan), 40 ng/mL basic fibroblast growth factor (PeproTech, Rocky Hill, NJ), 20 ng/mL epidermal growth factor (PeproTech), 2% B27 supplement (Life Technologies), and 5% fetal bovine serum. A total of 3–5 × 10^6 HEK at passage 2~5 and human DFs at passage 2~5 were mixed with 300–1000 human DP spheroids to prepare a cell slurry in a total volume of 150–200 uL of Epilife Basal Medium. The cell slurry was transferred onto a PET membrane and incubated for 1–2 h at 37°C, followed by grafting onto the back skin of a hairless NOD/SCID mouse, as previously described. Two to three months after

grafting, reconstituted skin tissues were collected. For preparation of paraffin-embedded samples, collected tissues were fixed overnight in Superfix KY-500 (Kurabo, Osaka, Japan), followed by dehydration and infiltration with paraffin using an automated processor, and manual embedding in paraffin wax molds. For preparation of frozen samples, collected tissues were fixed overnight in 4% paraformaldehyde in phosphate-buffered saline, processed in a sucrose gradient up to 30%, embedded with OCT compound (Sakura, Tokyo, Japan), and prepared as frozen blocks. Animal procedures were approved by the Ethics Committee of Shiseido Research Center in accordance with guidelines of the US National Institutes of Health (Bethesda, MD).

Histological staining

Paraffin block samples were sectioned (4 μm thick) and stained with hematoxylin and eosin. *In situ* hybridization (ISH) was performed with a human Alu-DNA-specific probe using the Ventana Discovery XT system according to the manufacturer's instructions (Roche). For double staining of human Alu-DNA and hair shafts, ISH was performed to detect human Alu-DNA with an Alexa488 antibody (Life Technologies), followed by immunohistochemical staining using a mouse monoclonal AE13 antibody (Abcam Cambridge, UK) and Alexa594 antibody (Life Technologies) according to

conventional procedures. For pan-cytokeratin staining, 7-μm thick frozen sections were incubated with a polyclonal rabbit anti-pan-cytokeratin antibody (Diagnostic BioSystems, CA) and Alexa488 antibody.

Tracking of injected human DSC in reconstituted skin

Human DSC cells were expanded from explant cultures in Amniomax C100 complete medium or MesenPRO RS medium (Life Technologies). After transfection with LV-CMV-EGFP vector (Sirion Biotech, Martinsried, Germany) overexpressing EGFP at MOI100, 3–5 × 10^6 fluorescent green-labeled human DSC cells were injected into reconstituted human skin with hair using a 27G needle. Injected reconstituted skin tissue was collected and processed for paraffin embedding and subsequent sectioning. Immunohistochemical staining for EGFP was performed using polyclonal rabbit antibodies against EGFP (MBL, Nagoya, Japan) and Alexa488.

II-2. 3 Results

CHIR99021 increased expression of dermal papilla signature genes

Compared with controls (Fig. 2-2-1a), human DP cells cultured with the Wnt signaling activator CHIR99021 (Fig. 2-2-1b) exhibited different cell morphologies with more prominent stress fibers. Expression levels of DP signature genes such as LEF1, versican, BMP4, Sox2, and noggin were measured in CHIR99021-stimulated DP cells using qRT-PCR (Fig. 2-2-1c). Expression of LEF1, BMP4, Sox2 ($P < 0.001$), and noggin ($P<0.05$) were significantly increased by CHIR99021 stimulation. However, expression of versican was not significantly altered.

CHIR99021 and 3D-spheroid culture synergistically enhanced dermal papilla signature gene expression

To generate 3D DP spheroids, three different methods were employed: self-aggregation using a SCIVAX NanoCulture dish (Fig. 2-2-2a), U-bottom method using an EZ-sphere dish (Fig. 2-2-2b), and floating drop using an Elplasia dish (Fig. 2-2-2c). DP spheroids were well formed by all methods, and were collected at 72 hr after seeding. To assess which method most enhanced the hair-inducing ability of DP cells, expression levels of LEF1, versican, BMP4, Sox2, and noggin [60, 65, 66] were measured using qRT-PCR (Fig. 2-2-2d). All 3D spheroid culture methods significantly increased the

expression of most genes examined. Most significantly, 3D spheroids generated by floating drop using Elplasia exhibited the highest expression of LEF1, versican, Sox2, and noggin, indicating that this method most effectively restored the intrinsic character of DP cells. Next, we assessed the synergistic interaction of CHIR99021 and 3D-spheroid culture by floating drop on DP signature genes expression (Fig. 2-2-2e). CHIR99021-stimulated 3D spheroids (Fig. 2-2-2g) exhibited a rougher surface compared with unstimulated 3D spheroids (Fig. 2-2-2f). Two-way ANOVA indicated a significant interaction between CHIR99021 stimulation and 3D-spheroid culture on expression of versican, Sox2, and noggin, with highest expression levels observed in CHIRR9021-stimulated 3D spheroids (Fig. 2-2-2e). These results indicated a synergistic increase of versican, Sox2, and noggin. Although this synergistic increase was unable to reach significance for expression of LEF1 and BMP4, the highest expression levels of these factors occurred in CHIRR9021-stimulated 3D spheroids. These results indicated that the hair-inducing ability of Elplasia-generated and CHIR99021-stimulated 3D DP spheroids was the most promising. To understand the mechanism of increased expression of DP signature genes in Elplasia-3D spheroids, we observed the aggregation process in floating drop using an Elplasia dish and compared gene expression levels of DP spheroids at different time point after seeding. 3D spheroids were already formed within 12–13 h after

seeding on Elplasia dish, and cells were observed to be moving within formed spheroids, which were constantly rotating during aggregation process (data not shown). Expression of versican, BMP4, Sox2, and noggin in 3D DP spheroids at 72 h after seeding was significantly increased compared with spheroids at 24 h after seeding (Fig. 2-2-3), indicating a time-dependent increase.

CHIR99021 and 3D-cultured DP spheroids contributed to hair follicle formation in reconstituted human skin

Our studies showed that the hair-inducing ability of Elplasia-generated and CHIR99021-stimulated 3D DP spheroids was the most promising. However actual hair-inducing ability was unknown. To assess the hair follicle-inducing ability of CHIR99021-stimulated 3D DP spheroids, an *in vivo* "Reconstituted skin assay" was employed by modifying an original method that used for murine cells [67]. Two to three months after grafting of cells (i.e. a slurry composed of human epithelial cells, dermal fibroblasts, and CHIR99021-stimulated spheroids) onto hairless NOD/SCID mice, hair shafts and raised skin were clearly observed (Fig. 2-2-4a). Hematoxylin and eosin staining revealed newly formed hair follicles and skin, which were continuous with host mouse skin (Fig. 2-2-4b, c). To investigate the origin of cells composing the newly generated skin, localization was assessed by *in situ* hybridization with a human Alu-DNA specific probe on sections

of generated skin. The results indicated generated skin was composed mostly by grafted human origin cells (Fig. 2-2-4d, e). In addition, AE13 antibody-positive hair shafts were surrounded by human Alu-DNA-positive hair follicles (Fig. 2-2-4e), indicating the formation of human hair follicles. Although grafting of human DP cells generated hair follicle-like structures in a previous report, human DP cells were found to be excluded around hair follicles [68]. To assess the contribution of CHIR99021-stimulated DP spheroids on formation of human hair follicles, the fate of DP spheroids was tracked. Two to three months after grafting of cell slurry containing DP spheroids labeled with the red fluorescence agent PKH26 (Sigma-Aldrich, St. Louis, MO) (Fig. 2-2-4g), red fluorescence-positive cells were observed in the DP and sheath cup of hair follicles (Fig. 2-2-4h,i), indicating the contribution of CHIR99021-stimulated DP spheroids to hair follicle formation. These results showed that successful *de novo* generation of reconstituted human skin with enriched hair follicles using CHIR99021-stimulated DP spheroids.

Functional evaluation of reconstituted human skin and hair follicles

Finally, to evaluate the functional features of reconstituted human skin and hair follicles, injection of human DSC cells into mice was performed. To track injected DSC

cells, human DSC cells were transfected with lentivirus overexpressing EGFP; successful labeling of DSC cells with green fluorescence was confirmed (Fig. 2-2-5a, b). Two weeks after intradermal injection into reconstituted skin, congregated DSC cells were observed in the dermis and subcutaneous tissue of reconstituted skin (Fig. 2-2-5c). Two to three months after injection, labeled DSC cells were observed in the dermal sheath (Fig. 2-2-5d), dermal sheath cup (Fig. 2-2-5e, f) of hair follicles. Notably, a substantial number of DSC cells were observed in the DSC of miniature hair follicles (Fig. 2-2-5e). These localization data are consistent with a previous report describing injection of mouse DSC cells into mouse skin [40]. After plucking hairs, newly formed hairs appeared, indicating the existence of hair cycling (data not shown). Collectively, these results indicated that generated human hair follicles in reconstituted skin were functional.

II-2. 4 Discussions

In present study, after optimization of DP cell culture condition for restoring expression of DP signature genes, we finally succeed *de novo* generation of reconstituted human skin with enriched hair follicles using CHIR99021-stimulated 3D spheroids. Our results showed that CHIR99021 stimulation increased expression of DP signature genes. Stress fibers were more prominent in CHIR99021-stimulated monolayer DP cells compared with controls (Fig. 2-2-1a, b), indicating actin cytoskeletal rearrangements were affected by alterations in Wnt signaling, as previously reported [69]. The surface of formed spheroids stimulated by CHIR99021 appeared rougher compared with unstimulated control spheroids (Fig. 2-2-2f, g), which may also be caused by cytoskeletal rearrangements induced by CHIR99021. Our results showed that 3D-spheroid culture and CHIR99021 stimulation could synergistically increase expression of DP signature genes with significance, indicating synergistic restoration of the intrinsic character of DP cells (Fig. 2-2-2e). Based on the results of gene expression profiling comparing human 3D spheroids with intact DP, expression levels of some factors in the Wnt signaling pathway could not be restored, even in 3D spheroids [64]. To elucidate whether combination of CHIR99021 stimulation and 3D-spheroid culture could fully restore the intrinsic character of DP cells, further exhaustive gene expression profiling is needed. With regard

to expression of assessed genes, LEF1 and BMP4 were not synergistically increased by CHIR99021 and 3D-spheroid culture. Instead, expression of LEF1 and BMP4 were increased consistently by CHIR99021 stimulation in both monolayer and 3D spheroids (Fig. 2-2-2e), indicating that the Wnt activator CHIR99021 is a robust regulator of BMP4 and LEF1 expression, regardless of morphological features. Indeed, expression of LEF1 is known to be directly regulated by Wnt signaling.

Differences in DP-related gene expression levels among the different 3D-spheroid culture methods were observed (Fig. 2-2-2d), indicating that different aggregation processes involved in each method could affect the restoration of DP cells, even if morphological features of 3D spheroids formed by each method are similar. The driving force of aggregation in each method is different, such as natural gravity with low- or no-attachment dishes (U-bottom and floating drop), and spontaneous cell-to-cell adhesion caused by a limited cell-attachment surface on SCIVAX NanoCulture dish. In addition, different frictional forces work to rotating formed spheroids between U-bottom and floating drop methods. As a result, these different physical properties affect the spheroid generation process, and may underlie differences observed in gene expression.

Despite the fact that 3D spheroids formed after 12–13 h seeding in aggregation, expression of DP genes in 72-hr incubated spheroids was increased compared with 24-hr

incubated spheroids (Fig. 2-2-3). In addition, active movement of composed cells within formed spheroids was observed (data not shown). These results suggest maturation of formed spheroids occurred with rearrangement of composing cells.

Based on the highest expression of DP signature genes, CHIR99021-stimulated DP spheroids generated by the floating drop method were the most promising to have hair-inducing ability (Fig. 2-2-2); indeed, these spheroids contributed to hair formation (Fig. 2-2-4). Although histological studies showed well-formed skin mainly composed of transplanted human cells, further histological studies are needed to verify them as humanized skin, such as investigating the localization of host mouse cells and also skin appendages other than hair follicles. To determine whether CHIR99021-stimulated DP spheroids were necessary for hair formation, grafting experiments of the cell slurry composed only by epithelial cells and dermal fibroblasts without spheroids were performed in a few mice (data not shown). Although generated reconstituted skin had no hair or only sparsely formed hair, further grafting experiments using a larger number of mice are needed to elucidate necessity. Recently, a reconstituted human skin assay to establish full thickness human skin with enriched hair follicles was reported [70]. In this assay, cultured cells isolated from fresh fetal scalp skin tissues have mainly been used as a material. Our generated humanized skin with enriched hair follicles could be a useful

model to study the mechanisms underlying human disease, or any physiological phenomenon in humans.

Injected human DSC cells were found in dermal sheath and dermal sheath cup of hair follicles (Fig. 2-2-5d-f), consistent with previous studies using mouse DSC cells. Interestingly, substantial DSC cells were observed in the DSC of miniaturized (vellus) hair follicles (Fig. 2-2-5e), implying the degree of contribution of injected DSC cells might be different in conditions of individual hair follicle or the stages of hair cycle. However, further histological studies are needed to elucidate whether the contribution of DSC cells to differentiate into DP is significant. As localization of injected DSC cells in dermal sheath including dermal sheath cup, was confirmed, and newly formed hairs appeared after plucking hairs, functional features of reconstituted skin and hair follicles generated in this experiment were verified. These results also indicate the usefulness of reconstituted human skin for the assessment of cell-based therapies for skin and hair disease. As described in CHAPTER I.5, the thickness of dermis and epidermis are different between mice and humans, and the hair size and hair cycle periods also differ. These differences could obfuscate investigation of the cell's behavior in xenotransplantation cases, such as when human cells are injected into mouse skin. Our generated humanized skin with enriched hair follicles could be used as a powerful model

to study the behavior of cutaneous injected cell-based therapies. In fact, human DSC cells have been assessed in our generated humanized skin and then injected human DSC cell were observed in the hair follicle, which is consistent with the results of a previous mouse study [40]. Further histological studies are needed to assess the contribution of injected DSC cells to regenerate the hair follicle but our studies showed that there is potential for human DSC cells to be used as part of a cell-based therapy for alopecia.

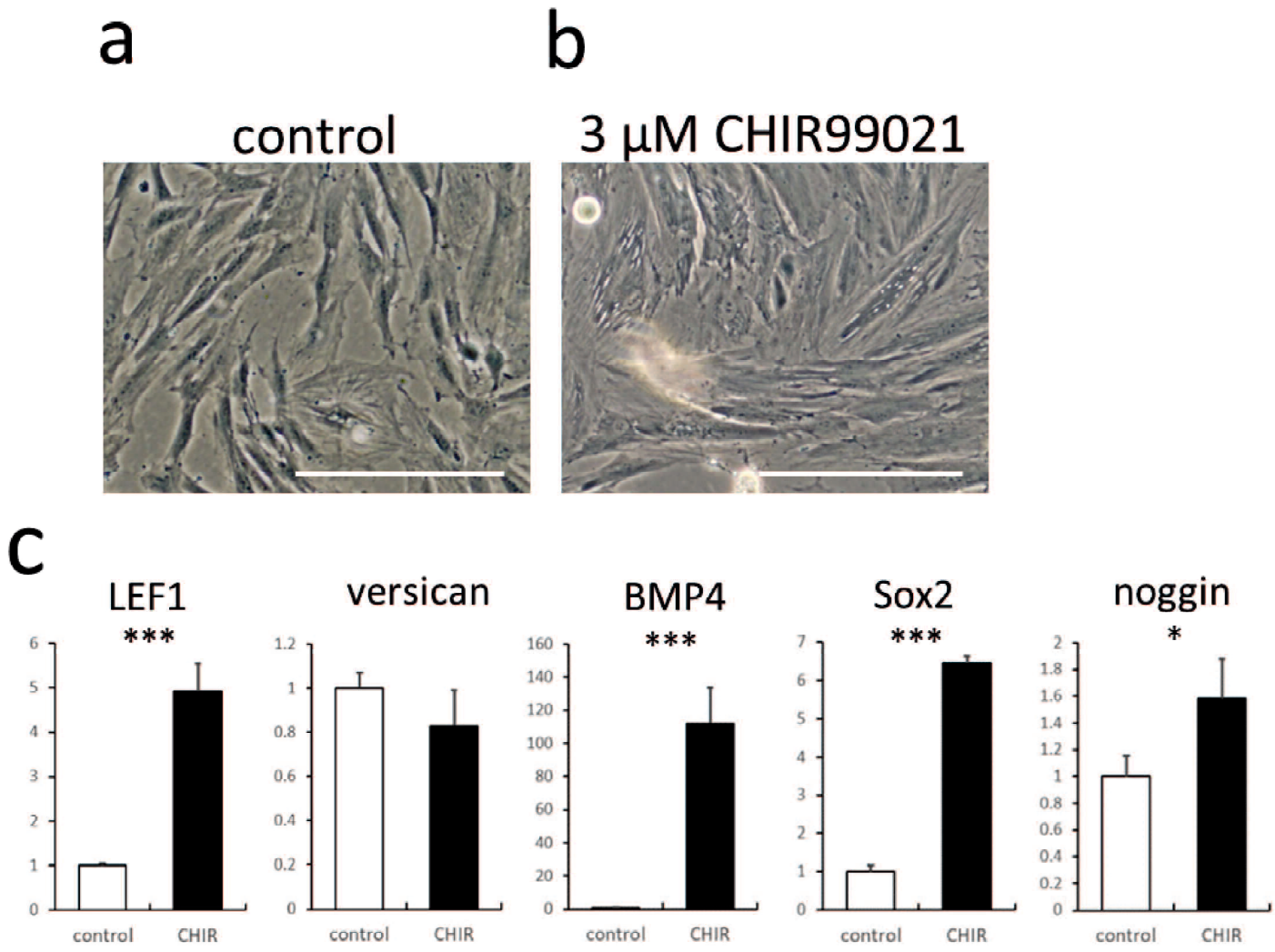

Figure 2-2-1. CHIR99021 increased expression of dermal papilla (DP) signature genes

Representative images of (a) monolayer-cultured DP cells and (b) DP cells cultured with 3 μM CHIR99021 for 72 h. (c) qRT-PCR analyses of DP signature genes, LEF-1, versican, BMP4, Sox2, and noggin in DP cells (control) and DP cells cultured with 3 μM CHIR99021 (CHIR) (n = 3). Input was normalized to GAPDH and results are expressed as mean ± S.D. Results are also expressed as fold change in each sample over control DP cells. Student's t-test was applied for comparison between control and CHIR. * $P < 0.05$, ***$P < 0.001$. Bars: 100 μm in a, b.

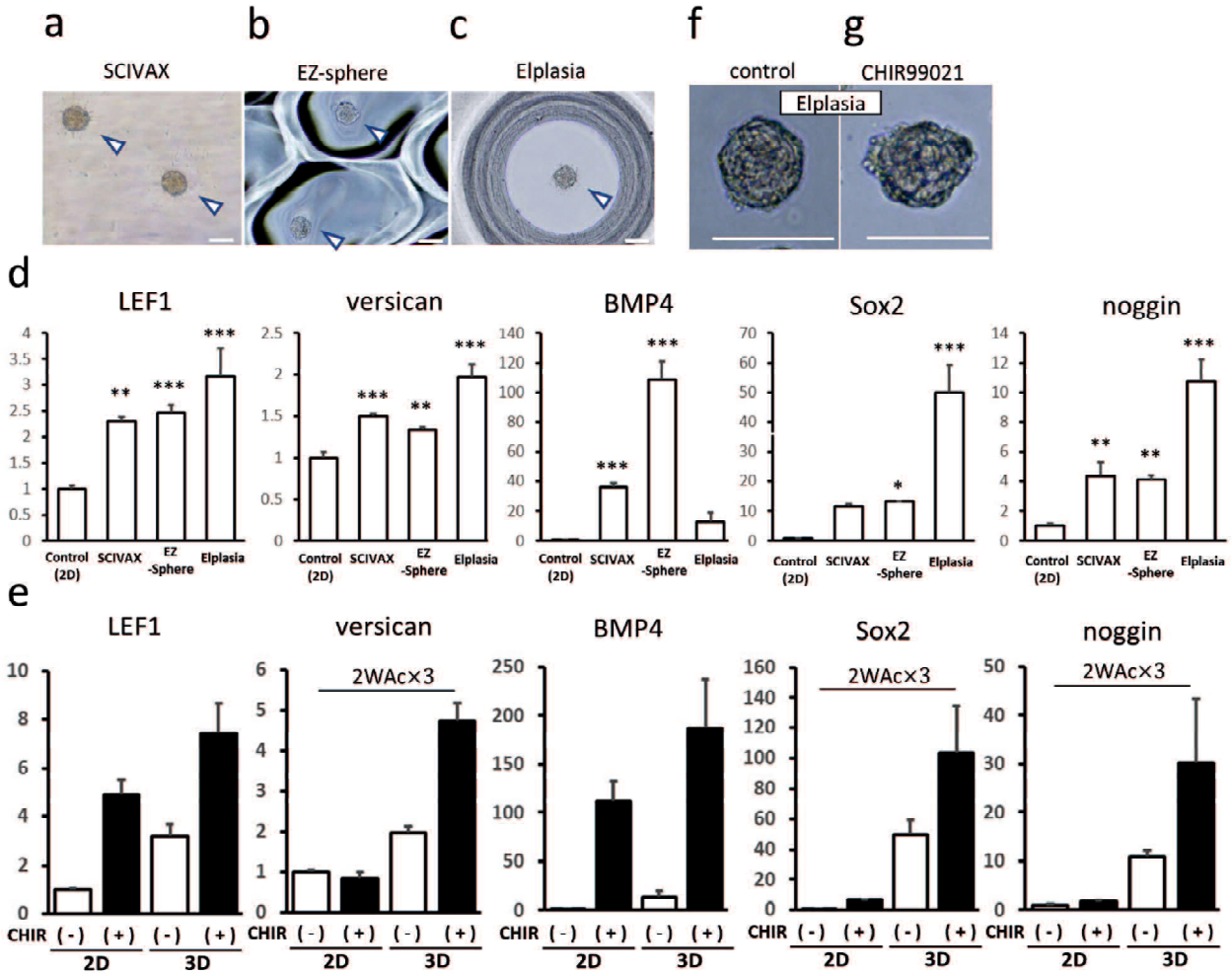

Figure 2-2-2. Comparison of three different 3D aggregation culture methods indicated increased expression of dermal papilla (DP) signature genes occurred synergistically with CHIR99021 stimulation

Representative images of aggregation-cultured DP spheroids using SCIVAX (a), EZ-sphere (b), or Elplasia (c). DP spheroids were collected at 72 h after seeding. Magnified images of spheroids prepared using Elplasia (f) and stimulated with 3 μM CHIR99021 (g). Arrowheads in a-c indicate aggregated DP spheroids. (d, e) qRT-PCR analyses of DP signature genes, LEF-1, versican, BMP4, Sox2, and noggin. Results are expressed as mean ± S.D. Input was normalized to GAPDH. (d) Comparison of expression levels of DP signature genes in monolayer DP cells (control, 2D) and DP spheroids using indicated vessels (n = 3). Results are expressed as fold change in each sample over 2D controls. Dunnett's multiple test was employed to compare with 2D controls. * $P < 0.05$, ** $P < 0.01$, ***$P < 0.001$. (e) Expression levels of DP signature genes in monolayer DP cells (2D) and DP spheroids (3D) prepared using Elplasia and cultured with (black bars) or

without (open bars) 3 µM CHIR99021 (n = 3). Results are expressed as fold change in each sample over 2D controls without CHIR99021. Two-way ANOVA indicated a significant synergistic interaction between CHIR99021 stimulation and 3D culture (2WAc×3). $P < 0.05$. Bars: 100 µm in a–c, f, g.

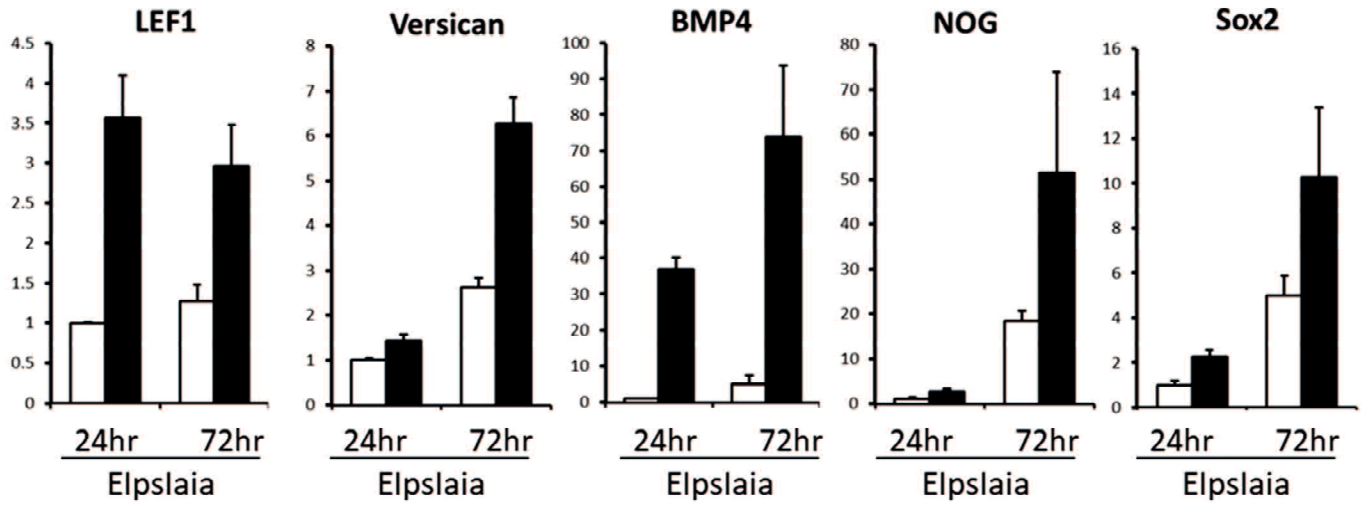

Figure 2-2-3. Incubation of aggregated dermal papilla (DP) cells elicited increased expression of DP signature genes

qRT-PCR analyses of DP signature genes LEF-1, versican, BMP4, Sox2, and noggin in DP spheroids (prepared using Elplasia) at 24hr and 72hr after seeding with 3 μM CHIR99021 (black bars), or without CHIR99021 as control (open bars) (n = 3). Input was normalized to GAPDH, and results are expressed as mean ± S.D. Results are also expressed as fold change in each sample over DP spheroids at 24hr after seeding without CHIR99021.

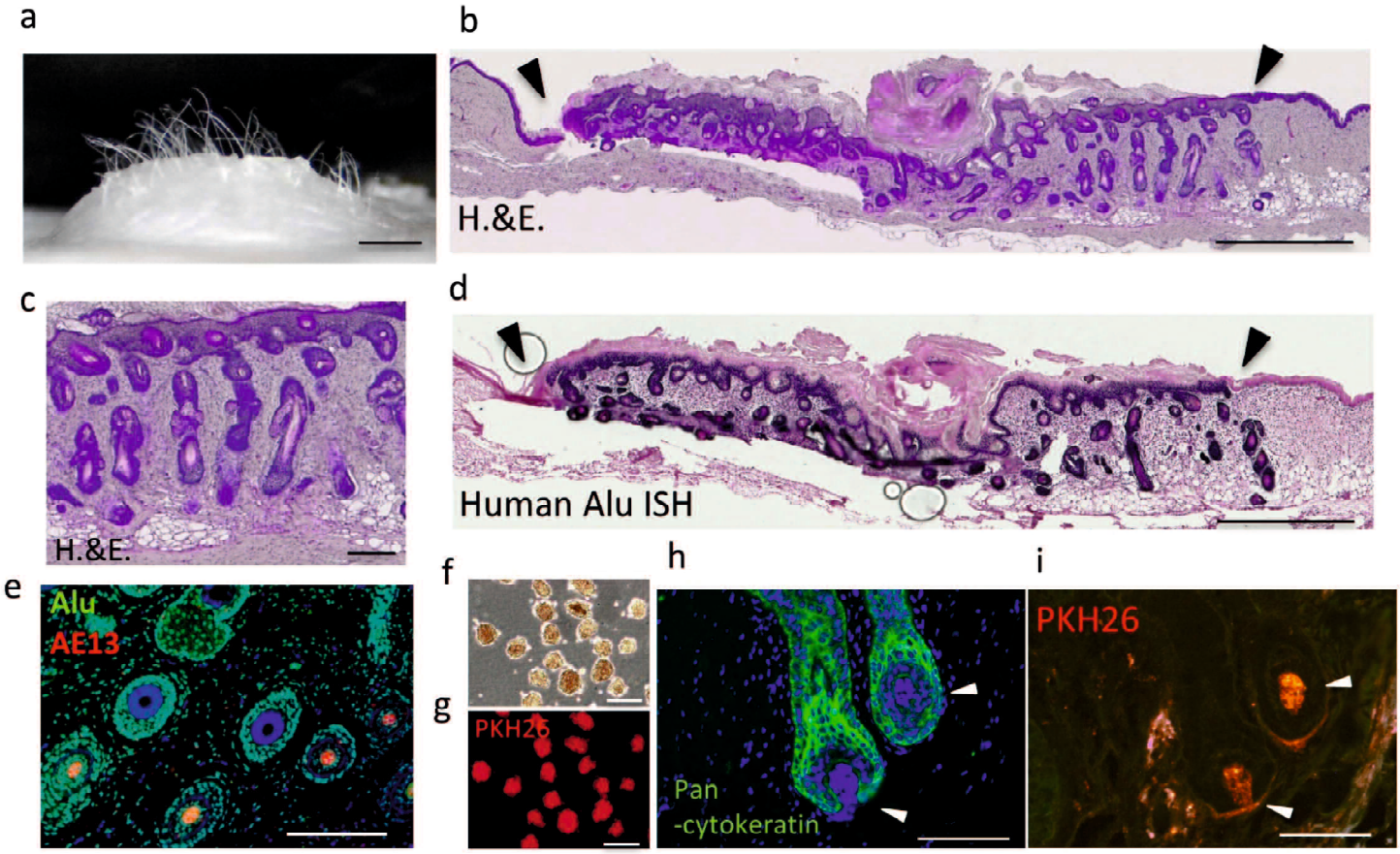

Figure 2-2-4. CHIR99021-stimulated dermal papilla (DP) spheroids contributed to hair follicle formation in reconstituted human skin

(a) Representative image of reconstituted human skin with hair generated by grafting of human cell mixtures including CHIR99021-stimulated DP spheroids prepared by Elplasia. (b, c) Hematoxylin and eosin stained sections. (d) Human Alu probe *in situ* hybridization (ISH) staining with chromogenic detection with BM purple. (e) Double staining of human Alu-DNA probe (from ISH staining) with fluorescence detection of Alexa488, and immunohistochemistry of a hair shaft marker AE13 antibody detected by Alexa594. Arrowheads in b, d indicate the border between reconstituted human skin and host mouse skin. (f, g) Image of PKH26-labeled DP spheroids prepared using Elplasia. (i) Localization of PKH26-labeled DP spheroids in reconstituted skin. (h) Sequential section of the section shown in i immunohistochemically stained with pan-cytokeratin and detected with Alexa488. Arrowheads in h, i indicate DP and DSC region where contributed DSC cells were localized. Bars: 200 μm in c, e–i; 1 mm in a, b, d.

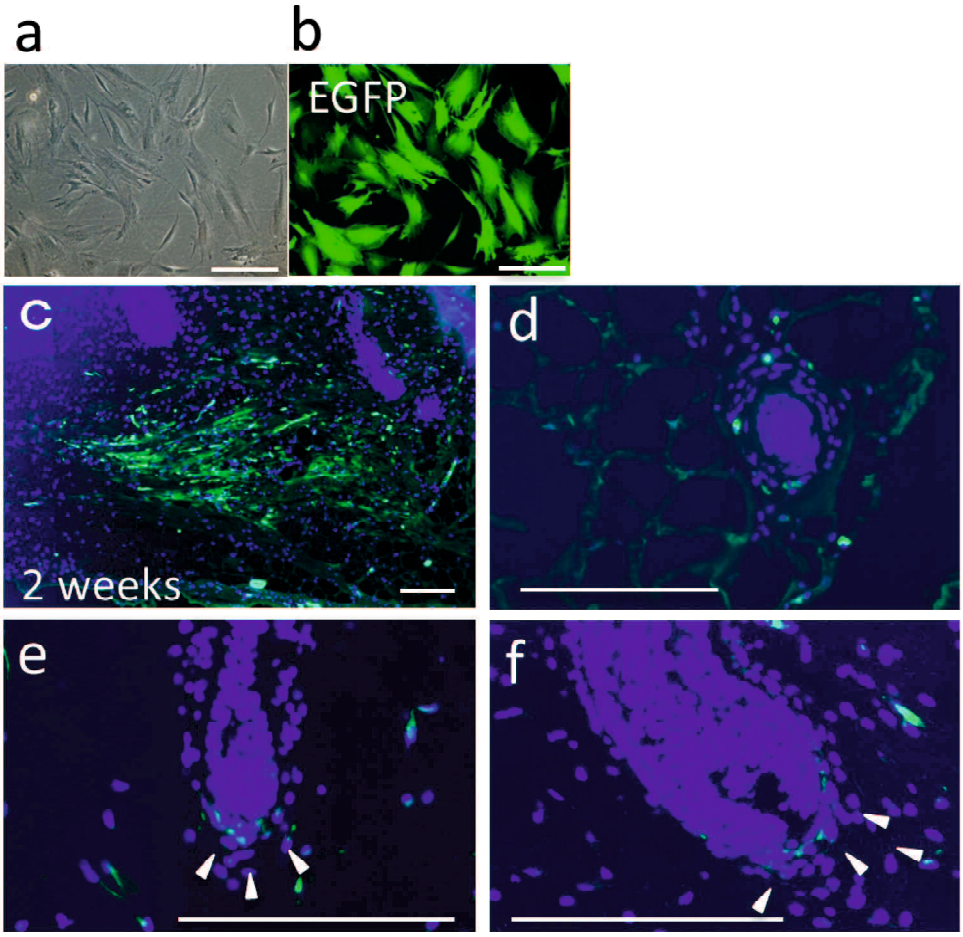

Figure 2-2-5. Analyses of injected dermal sheath cup (DSC) cells in reconstituted human skin with hair follicles

(a, b) Representative images of DSC cells transfected with an enhanced green fluorescent protein (EGFP)-overexpressing lentivirus vector. Localization of injected EGFP-labeled DSC cells at (c) 2 weeks and (d-f) 2 months after injection into reconstituted human skin with hair follicles. Injected DSC cells were observed in the dermal sheath region in transvers section of hair follicles (d), at DSC region of miniature hair follicles (e) and DSC region of hair follicles (f). Arrowheads in e, f indicate injected DSC cells localized at the DSC region. Bars: 200 μm in a-f.

CHAPTER III: Histological studies of cellulite and molecular mechanisms leading cellulite

III. 1 Background and objective

Cellulite is a chronic skin condition that is characterized by dimpling and lumpiness of the skin on the thighs, hips and buttocks. In colloquial speech, it is known as "orange peel skin". Cellulite does not affect a significant number of men but it affects the majority of women and often represents a major cosmetic and psychological concern. It has been suggested that the incidence of cellulite correlates with the body mass index (BMI) [71] but also women with a low/normal BMI (BMI: 18–25) frequently show the appearance of cellulite [72]. Thus, cellulite is not simply caused by overweight or obesity, but other, thus far unknown factors apparently contribute to its pathogenesis.

Since the exact mechanisms and causes of cellulite formation have not yet been determined, there are at present a large number of conflicting hypotheses regarding causative factors, including hormones, altered fat metabolism, lipodystrophy, modified blood circulation, abnormally shaped and less flexible connective tissue, and inherent factors such as race and genetic predisposition [73, 74]. These conflicting hypotheses arise from the paucity of scientific studies that have addressed the manifestation and development of cellulite symptoms.

Using magnetic resonance imaging (MRI), it was suggested that protrusion of adipose tissue into the dermis represents a characteristic feature of cellulite [72, 75]. The

protrusion of adipose tissue was also investigated by two other imaging technologies, *in vivo* confocal microscopy and high-resolution ultrasound [71], and it was consistently observed by several research groups. Apart from this finding, however, there is little consistency in the imaging observations because of the limitations of each noninvasive imaging technology. This indicates the necessity for detailed pathohistological analyses as well as for improved noninvasive imaging technologies.

Previously, a histological study of cellulite reported that the structures of fibrous strands (septa) in the subcutaneous tissue are modified in cellulite [76]. This finding was confirmed using MRI with quantitative analyses [75]. Abundant deposits of acid proteoglycan and alpha-2-macroglobulin were found in the septa in cellulite, which might influence the function of these septa in the subcutaneous tissue [76]. It is of interest that Pierard *et al.*, investigating the protrusion of adipose tissue, observed that the skin of women, regardless of whether the women showed the appearance of cellulite or not, exhibited a 'wavy' dermohypodermal junction formed by the protruding adipose tissue. This was in contrast to the smooth dermohypodermal junction seen in the skin of men [76]. It was also reported that striae, comprising strands of sclerotic collagen fibers, in the skin of women with cellulite penetrated into the papillary dermis; a finding that was not seen in male skin without cellulite.

The current study sought to comprehensively investigate the histological symptoms of cellulite, with a focus on the dermis and epidermis rather than the subcutaneous tissue, to identify additional features of cellulite and molecules that might participate in the development of cellulite. We performed the largest ever histological and immunohistological studies in 25 females with cellulite, 19 females without cellulite, and five males without cellulite, to determine characteristic symptoms of cellulite. We also investigated the expression levels of major extracellular matrix-related genes using qRT-PCR, and used transcriptional profiling of whole skin lysates and of dermal fibroblasts isolated by laser capture microdissection (LCM) to identify molecules potentially involved in the pathogenesis of cellulite.

III. 2 Material and methods

Human skin biopsies

Skin specimens were obtained from the lower buttocks or thighs of 49 volunteers (aged 19–67 years) with the approval of the ethics committee of the University Hospitals Case Medical Center. Skin biopsies (two 6-mm-punch biopsies per individual, including the epidermis, dermis and the upper part of the subcutaneous tissue) were obtained under local anesthesia from 25 females with cellulite, 19 females without cellulite (female controls), and five males without cellulite (male controls). The diagnosis of cellulite was made by a board-certified dermatologist. For each set of biopsies, one specimen was immediately frozen in liquid nitrogen and used for LCM, microarray analysis and qRT-PCR. The other specimen was embedded into optimal cutting temperature compound (Sakura FineTechnical, Tokyo, Japan) for histological and immunohistological analyses.

Histological stainings

Frozen skin samples were sectioned (7 μm thick) and stained with hematoxylin and eosin. We compared rete ridge scores among the different groups using digital images and Photoshop CS2 (Adobe, San Jose, CA). Two individual fields of view of the epidermis, 850–900 μm in width, were selected randomly in each section. The straight

length between each edge of the epidermis and the length of the basement membrane were measured. The length of the basement membrane was then divided by the measured straight length of the epidermis, providing a rete ridge score, which reflects the frequency and depth of rete ridge structures. Additional sections were subjected to picrosirius red staining, elastica van Gieson staining and several histochemical stains. For detection of hyaluronan (hyaluronic acid), sections were incubated with 3% H_2O_2 in anhydrous methanol for 45 min at room temperature to block endogenous peroxidase activity, and then washed in phosphate-buffered saline (PBS) twice. After blocking nonspecific binding by incubation with 0.1% bovine serum albumin in PBS for 1 h at room temperature, sections were incubated with 2 μg/mL biotinylated hyaluronic acid binding protein (Associates of Cape Cod, East Falmouth, MA) in blocking solution for 90 min. After washing three times with PBS, sections were incubated with streptavidin Alexa Fluor 594 conjugate (Invitrogen, Carlsbad, CA) in blocking solution for 1 h. After washing three times with PBS, sections were mounted with Vectashield mounting medium (Vector Laboratories, Burlingame, CA). Sections were examined with an Axioskop 2 MOT plus microscope (Carl Zeiss, Oberkochen, Germany), equipped with an AxioCam MRc camera. Images were acquired using AxioVision software 4.7.1 (Carl Zeiss).

Laser capture microdissection

Five cellulite specimens and five female control specimens were subjected to LCM. All procedures were performed so as to minimize RNase contamination, using the appropriate grades of solutions and equipment and RNaseZap (Ambion, Austin, TX). Skin samples were embedded into optimal cutting temperature compound, and 7-μm-sections were cut and placed on polyethylene naphthalate membrane slides (Molecular Devices, Sunnyvale, CA). Slides were stained using a frozen section staining kit (Arcturus, Mountain View, CA) according to the manufacturer's protocol. After sequential dehydration steps, sections were dried for 2–3 min in a hood. LCM was performed using a Veritas microdissection instrument (Arcturus) with CapSure HS LCM caps (Molecular Devices). The papillary and upper reticular dermis (an area at about 1-mm-depth from the epidermis), where only single cell fibroblasts were located, were cut with a UV laser and captured. Optimized settings for capture were 70–75 mW pulse power, 2.5 ms pulse duration, and 25–45 μm spot diameter. The power of the cutting laser was set at low level (2–5%). For each specimen, single cells were captured from a total dermal area of 10–15 mm^2 and were collected from eight to 12 sequential sections. Captured cells were incubated with Buffer RLT plus (Qiagen, Hilden, Germany) containing beta-mercaptoethanol for 30 min at 42°C. RNA was extracted and purified

from the homogenized captured cells using a RNeasy Plus Micro kit (Qiagen) according to the manufacturer's protocol.

Gene microarray analyses

Amplification of RNA and conversion to single-stranded cDNA was performed using the Whole Transcriptome-Ovation Pico RNA Amplification System (NuGEN Technologies, San Carlos, CA). The quality and quantity of the single-stranded cDNA was determined using a NanoDrop ND 1000 (NanoDrop, Wilmington, DE) and a Bioanalyzer 2100 (Agilent Technologies, Santa Clara, CA).

Single-stranded cDNA (3.5 μg) was converted into sense target cDNA using the WT-Ovation Exon Module (NuGEN Technologies). Fragmented and biotin-labeled sense target cDNA was generated using the Encore Biotin Module (NuGEN Technologies). Biotin-labeled single-stranded cDNA targets (4.7 μg) were mixed in 220 μL of hybridization mix (Affymetrix, Santa Clara, CA) containing a hybridization control and control oligonucleotide B2 (Affymetrix). Samples were hybridized to GeneChip Human Exon 1.0 ST arrays for 18 h at 45°C. Arrays were then washed using an Affymetrix Fluidics Station 450 FS4500004 protocol. A GeneChip Scanner 3000 (Affymetrix) was used to measure the fluorescence intensity emitted by the labeled target. Background

correction, normalization, and summarization were performed using the robust multi-array average algorithm [77].

Differential expression in cellulite *vs.* female control samples was evaluated using Student's t-test. The relative expression of genes in cellulite *vs.* female control samples is expressed as a log2 ratio. Statistical significance was corrected for multiple testing using the Benjamini–Hochberg method. The probes designed for this exon array were filtered with a log2 signal threshold of 4.644.

Immunohistochemistry

Immunohistochemical staining for sarcoglycan-gamma and epidermal growth factor-containing fibulin-like extracellular matrix protein 1 (EFEMP1) was performed with 7-µm-thick frozen sections, fixed with 4% paraformaldehyde for 15 min, using monoclonal mouse antibodies against sarcoglycan-gamma (Abcam, Cambridge, UK) or EFEMP1 (Santa Cruz Biotechnology, Santa Cruz, CA) and a CSA II kit (DakoCytomation, Glostrup, Denmark) for chromogenic detection, according to the manufacturer's protocol. Nuclei were counterstained with hematoxylin.

For biglycan, fixed sections were incubated with Protein Block (DakoCytomation) for 30 min, followed by incubation with a polyclonal rabbit anti-biglycan antibody

(Sigma-Aldrich, St. Louis, MO) in antibody diluent (DakoCytomation) for 2 h. After three washes, sections were incubated with Alexa Fluor 594-conjugated anti-rabbit IgG in antibody diluent containing Hoechst 33342 (Invitrogen) for 1 h. Stained sections were mounted with Vectashield mounting medium. The extent of biglycan staining was graded independently by two observers in a blinded fashion using a score for the signal intensity (0, none; 1, weak; 2, moderate; and 3, strong).

Immunohistochemical stains for perilipin were performed with 20-μm-thick paraformaldehyde-fixed frozen sections using a polyclonal guinea pig anti-perilipin antibody (Progen, Heidelberg, Germany) and Alexa Fluor 594-conjugated anti-guinea pig IgG. The area of protruding adipose tissue was analyzed in perilipin-stained sections using Photoshop CS2. An area of 3 mm width × 4 mm depth (from the epidermis to the dermis) was randomly selected on the acquired images. The area of perilipin-positive adipose tissue and the total area of tissue were measured, and the percentage of total area covered by adipose tissue was used for comparison of the relative area of protruded adipose tissue among the different groups of samples.

RNA extraction from whole skin

RNA was extracted from 10 cellulite and nine female control samples, which were

from different donors than those used for LCM. After removal of the subcutaneous tissue with scissors, the remaining tissue was cut into small pieces in RNAlater RNA stabilization reagent (Qiagen). The minced tissue was soaked in RNAlater for 12 h at 4°C and then transferred into 2 mL tubes containing TRIzol (Invitrogen) and 5-mm stainless steel beads (Qiagen). Homogenization was performed using a TissueLyser (Qiagen). After insoluble debris was removed by centrifugation, RNA was extracted using a TRIzol plus RNA purification kit (Invitrogen) according to the manufacturer's protocol. cDNA was synthesized using a high capacity RNA-to-cDNA kit (Applied Biosystems, Foster City, CA) according to the manufacturer's protocol.

Quantitative real-time reverse transcription-polymerase chain reaction (qRT-PCR)

Expression of human biglycan, EFEMP1 and sarcoglycan-gamma was investigated using FastStart SYBR Green Master (Roche, Basel, Switzerland) and the AB 7900 HT Fast Real-Time PCR System (Applied Biosystems), or LightCycler 480 SYBR Green Master (Roche) and a LightCycler 480 II (Roche). Quantification of expression was performed using the $2^{-\Delta\Delta CT}$ method [50]. Relative expression levels were calculated using either glyceraldehyde 3-phosphate dehydrogenase (GAPDH) (for cDNA synthesized from whole skin-extracted RNA) or 18S rRNA (for cDNA synthesized from LCM-

captured RNA) as a reference gene. The primer pairs were designed as follows:

Primer sets used for qRT-PCR analyses

Gene name	Forward (5′ to 3′)	Reverse (5′ to 3′)
Biglycan	CAGAACAACGACATCTCCGAGC	ATCTCCACCAGGTGGTTCTTGG
EFEMP1	GCTTCCGTTGTTATCCACGAAATCC	CTGTATCTGGAAGATGTCTGATGGC
Sarcoglycan -gamma	GAGGCCAGAGAATCAGTATGTCTAC	CCATCTTTTGTTACACACAAGTGGCC
GAPDH	GAGTCAACGGATTTGGTCGT	TGGGATTTCCATTGATGACA
18S rRNA	CGGCTACCACATCCAAGGAA	GCTGGAATTACCGCGGCT
COL1A1	CAAGAGGAAGGCCAAGTCGAG	TCACAGATCACGTCATCGCACAAC
COL3A1	CATGGATCAGGCCAGTGGAAATG	CACAGCCTTGCGTGTTCGATATTC
COL12A1	GAGAAAGGTGAAAGGGGTACTGG	GGTCCTCGGATACCTGAGTTTC
Elastin	AGGAGCTGGGATTCCAGTTGTC	CTCCAACCCCGTAAGTAGGAATG
Fibrillin-1	CAGGAAACGGAGAAGCACAAACG	TGTAAGAGCTGGAAGGAGTTCTAGG
Fibulin-5	AAATGCATTGACCCCATCCGCTG	TGGCTTGCATTTGGAAGATGTCAGC
LOX	CTGGCTGTTATGATACCTATGGTGC	ATACGCATGATGTCCTGTGTAGCG
LOXL1	GCTGCTATGACACCTACAATGCG	GTTTGTTGCAGAAACGTAGCGACC
MMP1	ACGATCTATGGATCCAGGTTATCCC	GAACCAGCTATTAGCTTTCTGGAGAG
MMP2	AGAAGAAAATGGATCCTGGCTTCCC	GGATTTGATGCTTCCAAACTTCACGC
MMP3	GCCAGGGATTAATGGAGATGCC	GTCTGTGAGTGAGTGATAGAGTGG
MMP9	AATCCTACTCCGCCTGCACCAC	AAGTGAAGGGGAAGACGCACAG
TIMP1	ACCAGAAGTCAACCAGACCACC	AGCAATGAGAAACTCCTCGCTGC
TIMP2	AGAAGAAGAGCCTGAACCACAGG	CACTTCTCTTGATGCAGGCGAAG
TIMP3	GTGGGGAAGAAGCTGGTAAAGG	TACTGGTACTTGTTGACCTCCAGC

The designed primer pairs were verified by analyzing the melting curve with single amplicons.

The false discovery rate was controlled by correcting P-values using the Benjamini–Hochberg method.

III. 3 Results

Flattening of epidermal rete ridges in cellulite skin

Skin specimens were obtained from the lower buttocks or thighs of females without cellulite (n=19; Fig. 3-1a), of females with cellulite (n=25), exhibiting the characteristic dimpled appearance of the skin (Fig. 3-1b), and of males without cellulite (n=5). Hematoxylin and eosin stains of frozen skin sections revealed that epidermal rete ridges were shallower in cellulite skin (Fig. 3-1d) than in females without cellulite (Fig. 3-1c).

To quantify the morphological differences in epidermal rete ridges, we established a quantitative rete ridge score, which reflected the frequency and depth of rete ridges. We found that the rete ridge score was significantly lower in cellulite skin (score 1.38) than in female control skin (score 1.68; $p \leq 0.001$) or in male control skin (score 2.32; $p \leq 0.05$) (Fig. 3-1i). Since flattening of epidermal rete ridges might be associated with aging, rete ridge scores were plotted against age for each cellulite and female control skin sample. While there was a trend for reduced rete ridge scores with aging in normal skin ($r=-0.005$) and in cellulite skin ($r=-0.0016$) (Fig. 3-1j), rete ridges were shallower in cellulite than in female control skin for each age group. There was no major difference in epidermal thickness of cellulite *vs.* female control skin.

Pronounced changes of the extracellular matrix in the dermis of cellulite skin

We next assessed major components of the dermal extracellular matrix in cellulite skin by staining for collagen, elastic fibers and hyaluronan (hyaluronic acid). Sirius red staining revealed that the total amount of collagen in the entire dermis was not consistently different in cellulite (Fig. 3-1f) and female control skin (Fig. 3-1e). In Sirius red stainings, two distinct dermal layers, namely the upper papillary and the lower reticular dermis, could clearly be distinguished, based on the different arrangement and amount of collagen fibers [17]. We found that the papillary dermis was consistently thinner in cellulite skin (Fig. 3-1f) than in female control skin (Fig. 3-1e). Elastica van Gieson stains revealed an abundant elastic fiber network in the dermis of female control skin (Fig. 3-1g), whereas elastic fibers were scarce and disorganized in cellulite skin (Fig. 3-1h). In six out of 25 cellulite specimens, but not in normal control skin, areas of irregularly condensed collagen were observed, associated with absence of a well defined papillary dermis (Fig. 3-1k and l). Staining for hyaluronic acid revealed higher amounts of hyaluronic acid in the upper dermis than in the lower dermis, whereas there was no significant difference between cellulite and female control skin (Fig. 3-1m and n).

Protrusion of adipose tissue into the dermis of cellulite skin

We next assessed the distribution of adipose tissue within the skin, using immunohistochemical stainings for perilipin, a major adipocyte-specific phosphoprotein [78]. In normal skin, there was a clear distinction between the subcutaneous adipose tissue and the overlying dermis (Fig. 3-2a). In contrast, the subcutaneous adipose tissue drastically protruded into the dermis of cellulite skin (Fig. 3-2b), in agreement with previous observations obtained by noninvasive MRI [72, 75]. To quantify the differences in the amount of protruded adipose tissue, we measured the area occupied by adipose tissue in randomly selected dermal areas of 3 mm width × 4 mm depth (below the epidermal basement membrane). We found a significantly greater amount of protruded adipose tissue in cellulite skin (10.5% ± 1.1%, n=24) than in female control skin (5.0% ± 0.9%, n=18; p=0.001) or male control skin (3.9% ± 1.1%, n=4; p=0.03) (Fig. 3-2c).

Taken together, the histological analyses revealed shallower rete ridges, a reduced thickness of the papillary dermis, irregularly condensed collagen fibers, disorganized elastic fibers, and a greater amount of protruding adipose tissue in the dermis of cellulite skin. These findings suggested that cellulite might be associated with an impairment of dermal fibroblast functions since the structural features of the epidermal rete ridges may depend on the type and character of dermal fibroblasts [16], and since dermal fibroblasts also play an important role in the regular organization of the papillary dermis and the

dermal elastic fiber network. Moreover, modified subcutaneous adipocytes might impair the function of dermal fibroblasts [79, 80].

Expression of dermal extracellular matrix-related genes in cellulite skin

Based on the results of the morphological analyses, we next investigated the mRNA expression levels of major extracellular matrix-related genes, including collagens, elastic fiber components, LOX, LOXL1, fibulin-5, matrix metalloproteinases (MMPs) and tissue inhibitors of metalloproteinases (TIMPs) in whole skin extracts from cellulite and female control skin.

Type I, III and XII collagen represent the major collagens in human dermis [17], and type I and III collagen are enriched in adult skin [81]. We found that the mRNA expression levels of the type I collagen α1 (I) chain (COL1A1), COL3A1 and COL12A1 were not significantly different between cellulite and female control skin (Fig. 3-3). Elastin and fibrillin are major components of elastic fibers, and LOX, LOXL1, and fibulin-5 have essential roles in elastic fiber assembly [82]. The expression levels of elastin, fibrillin, fibulin-5, LOX and LOXL1 were not significantly different between cellulite and female control skin (Fig. 3-3). Analysis of the expression levels of MMPs and TIMPs revealed that expression of MMP1 was significantly decreased (P=0.007) in

cellulite compared with control skin and that there was a slight reduction of MMP3 expression (P=0.09) (Fig. 3-3). The expression levels of MMP2, MMP9 and TIMP 1–3 were comparable in cellulite and female control skin (Fig. 3-3).

Transcriptional profiling of dermal fibroblasts in cellulite skin

We next aimed to investigate the global transcriptional profiles of dermal fibroblasts in cellulite skin. To this end, we performed LCM to specifically isolate RNA from dermal fibroblasts, followed by gene microarray analyses. To predominantly capture dermal fibroblasts from frozen skin sections, we cut and used areas of tissue where only single fibroblast-like cells were located, but not vessels or skin appendages (Fig. 3-4a–d). Type I collagen is the major collagen within the dermis, and COL1A1 is synthesized and secreted by dermal fibroblasts. The expression of COL1A1 in captured tissue areas was analyzed using qRT-PCR and compared with expression levels in total skin (Fig. 3-4e). The expression of COL1A1 in the captured tissue of cellulite specimens was 20- to 120-fold higher than that in whole skin, indicating that the captured tissue was highly enriched in fibroblasts.

Laser capture of the dermal fibroblast-enriched area was performed on cellulite (n=5) and female control skin sections (n=5), followed by isolation of RNA, cDNA

amplification and gene microarray analyses. Gene expression analysis revealed several differentially expressed genes in captured fibroblasts from cellulite skin (Table 3). In particular, we found that expression of sarcoglycan-gamma (SGCG) (fold change: 0.55, P=0.014) and MMP2 (fold change: 0.61, P=0.036) was significantly down-regulated in fibroblasts from cellulite skin compared with female control skin, and that the expression of testis-specific Y-encoded-like protein 1 (TSPYL5; fold change: 1.44, P=0.027) and coiled-coil domain containing 45 (CCDC45; fold change: 1.35, P=0.012) was significantly up-regulated in cellulite fibroblasts. Although we found several other differentially expressed genes (Table 3) in the microarray analysis, the expression differences did not reach statistical significance.

Due to their potential roles in extracellular matrix production, the mRNA levels of sarcoglycan-gamma (SGCG), biglycan (BGN in Table 3) and EFEMP1 in the captured samples were also examined using qRT-PCR, biglycan (BGN) and EFEMP1 were found to be downregulated in the microarray analysis (Table 3). Although all three genes showed decreased mRNA expression levels in cellulite samples compared with control samples, the expression differences did not reach significance (Fig. 3-4f).

Reduced expression of biglycan, sarcoglycan-gamma and EFEMP1 proteins in cellulite skin

Biglycan is a member of a family of proteoglycans known as small leucine-rich proteoglycans [83]. Biglycan is widely expressed in the extracellular matrices of bones and of specialized, nonskeletal connective tissues [84], and mice deficient in biglycan display connective tissue anomalies of the bone and skin [85, 86]. To investigate whether the expression of biglycan is also down-regulated at the protein level in dermal fibroblasts of cellulite skin, immunohistochemical analyses for biglycan were performed.

In normal skin, biglycan was mainly detected in the papillary dermis, with the strongest expression immediately below the epidermis (Fig. 3-5a). By contrast, biglycan expression was greatly reduced in the dermis of cellulite skin (Fig. 3-5b). To quantify this observation, signal intensity scores were determined as shown in Figure 3-5c. The biglycan expression scores were significantly lower in cellulite skin than in female control skin (P=0.006) (Fig. 3-5d). Sarcoglycan-gamma is a transmembrane component of the dystrophin-associated protein complex that creates a mechanical linkage between the cytoskeleton and the extracellular matrix in muscle tissue [87]. Loss of sarcoglycan-gamma causes pronounced dystrophic muscle changes and membrane disruptions in muscle tissue [88, 89]. Little is known about its expression and role in nonmuscular tissues. Immunohistochemical analyses revealed expression of sarcoglycan-gamma in epidermal keratinocytes and dermal fibroblasts, as well as in smooth muscle cells of the

arrector pili muscle (Fig. 3-5e and f). Expression of sarcoglycan-gamma was decreased in cellulite samples (Fig. 3-5f) compared with female control skin (Fig. 3-5e), in particular, in papillary dermal fibroblasts (Fig. 3-5g and h).

EFEMP1, also known as fibulin-3, is an extracellular matrix glycoprotein of the fibulin family [90, 91]. EFEMP1 contributes to the integrity of elastic fibers in the connective tissue of fasciae and the vaginal wall, and lack of EFEMP1 causes inguinal hernias and pelvic prolapse [92, 93]. Immunohistochemical analyses of normal skin showed expression of EFEMP1 in the suprabasal layers of the epidermis and also co-localization with oxytalan and elastic fibers in the dermis (Fig. 3-6a, c, e, and g). Decreased EFEMP1 expression in this area was observed in cellulite samples (Fig. 3-6b and f), and oxytalan and elastic fibers were also decreased in cellulite samples (Fig. 3-6d and h). In fibrous septa within normal subcutaneous tissue, where a dense and robust elastic fiber network was observed, EFEMP1 largely co-localized with elastic fibers (Fig. 3-6i and k). In cellulite samples, EFEMP1 expression was reduced (Fig. 3-6j and l). We next investigated EFEMP1 expression levels by qRT-PCR with RNA isolated from whole skin lysates. We found that expression of EFEMP1 was significantly down-regulated in cellulite skin (fold change: 0.72, P=0.023) compared with normal control skin (Fig. 3-6m).

III. 4 Discussions

Mechanisms contributing to cellulite formation

The results of our histological study indicate that shallower rete ridges, a thinner papillary dermis, irregularly condensed collagen, disorganized elastic fibers, and greater amounts of protruded adipose tissue are key features of cellulite. Rete ridge flattening generally occurs with aging, as was also found in the present study. However, the cellulite-associated rete ridge flattening was independent of aging since rete ridges in cellulite samples were shallower than those in control samples in all age groups. Since regular formation of rete ridges depends on papillary fibroblasts [16], the shallower rete ridges observed in cellulite samples were most likely related to the significant thinning of the papillary dermis

A key finding of our study was the increased protrusion of adipose tissue into the dermis. Together with the reduction of elastic fibers and the thinning of the papillary dermis, this argues for a reduced function of the dermis as a cushion against fat protrusion, leading to the outward manifestation of ripples in the skin, a characteristic feature of cellulite. Even though noninvasive MRI studies have reported increased areas of adipose tissue protrusion into the dermis in cellulite [72, 75], a histological study found that protruding adipose tissue is a characteristic feature in female skin in general, regardless

of whether or not cellulite is observed [76]. In the present study, quantification of histological stains clearly revealed an increased protrusion of adipose tissue in cellulite samples compared with control samples but the differences between female and male control skin were minor.

A modified orientation [75] and uneven thickness of fibrous septa [75, 76] within the subcutaneous tissue have been previously detected in cellulite. In the hypodermis, fibrous septa do not only separate lobules of adipose tissue, but also connect the dermis to the underlying fascia. In the current study, we were unable to examine the structures of the fibrous septa in more detail as the 6-mm-biopsy tissue samples only included part of the subcutaneous tissue and fibrous septa. In some cellulite specimens, in which the papillary dermis was greatly diminished, we observed irregularly condensed collagen fibers, likely creating uneven physical properties in the skin. How these observations relate to the formation of cellulite will require further study. However, we found that the expression of MMP1 and MMP3 was significantly decreased in cellulite samples compared with female control samples. Since MMP1 and MMP3 are major collagenases of the dermis, decreased MMP1 and MMP3 levels may contribute to the observed irregularly condensed collagen.

Possible participation of extracellular matrix-related proteins in cellulite development

LCM and gene microarray analysis of dermal fibroblasts from cellulite and control skin identified several candidate modifier genes. Immunohistochemical analyses confirmed decreased expression of biglycan, sarcoglycan-gamma and EFEMP1 in cellulite. Biglycan deficiency in mice leads to structural abnormalities of collagen fibrils in the dermis and bone, and to thinning of the dermis [86]. Thus, decreased biglycan expression might contribute to the thinning of the papillary dermis in cellulite.

Mice lacking sarcoglycan-gamma develop membrane disruptions and have increased numbers of apoptotic cells in muscle tissue, resulting in pronounced dystrophic muscle changes [88]. To our knowledge, expression of sarcoglycan-gamma in cutaneous cells has not been reported previously. In the current study, we observed sarcoglycan-gamma expression in dermal fibroblasts in situ, and also observed a decrease of sarcoglycan-gamma expression in cellulite. It will be of interest to investigate, in future studies, whether decreased sarcoglycan-gamma levels might affect the membrane integrity or viability of dermal fibroblasts in cellulite.

A key finding of the present study was the significantly reduced expression of EFEMP1 in the dermis of cellulite, whereas the expression of major components and modulators of elastic fibers (elastin, fibrillin-1, LOX, LOXL1 and fibulin-5) did not

significantly change. Although mice lacking EFEMP1 show dermal elastic fiber abnormalities [92] , further studies will be required to determine, at least in part, whether decreased EFEMP1 expression contributes to the disorganized elastic fibers observed in the dermis of cellulite. In some tissue sections that included parts of the fibrous septa, decreased EFEMP1 expression in the fibrous septa was observed. The fibrous septa separate lobules of adipose tissue and serve as a protective padding to cushion the subcutis, as a physical partition. Our findings indicate the possibility that decreased EFEMP1 expression might contribute to the adipose tissue protrusion in cellulite, also known as 'fat herniation' due to less elastic fibrous septa that can no longer function as a partition. An altered orientation and uneven thickness of the fibrous septa have indeed been observed in cellulite and represent characteristic features of cellulite [75, 76].

Taken together, our analyses revealed characteristic structural and molecular features of the dermis in cellulite, indicating a more comprehensive involvement of the skin that goes beyond the established alterations of the subcutaneous adipose tissue in the development of cellulite. The detailed mechanisms how the identified extracellular matrix-associated proteins might contribute to cellulite pathogenesis, as well as their relevance as potential therapeutic targets will need to be investigated in future studies.

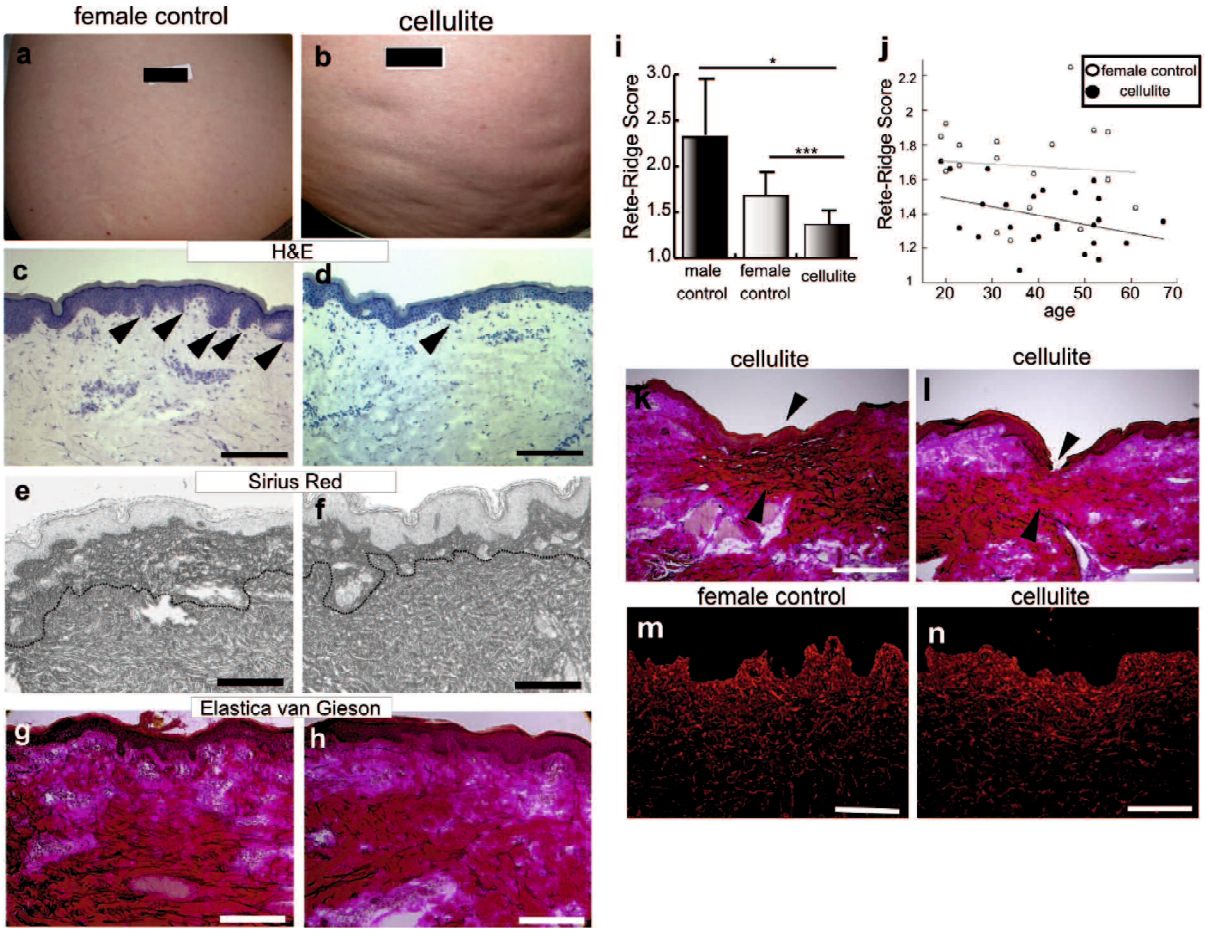

Figure 3-1. Comparison of cellulite and control skin samples

Photographs of the buttock skin of female control (a) and cellulite skin (b). Representative images of hematoxylin and eosin stained sections from female control (c) and cellulite samples (d). Well-formed rete ridge structures are indicated by arrowheads. Sirius red (collagen) stained sections from female controls (e) and cellulite samples (f). Representative black&white images of sections are shown. The black dashed line represents the boundary between papillary and reticular dermis. Note that the papillary dermis in the cellulite sample is thinner than in control skin. (g, h) Elastica van Gieson stained sections represent elastic fibers (black) and collagen (red). Representative images of sections of female controls (g) and cellulite samples (h) are shown. Disorganized elastic fibers are observed in the dermis of the cellulite sample. Bars: 200 µm (c-h). (i) The rete ridge score was calculated to assess the frequency and depth of rete ridge structures. Score values are expressed as mean ± SEM calculated from cellulite (n=24), female control (n=19), and male control samples (n=5). ***P<0.001. (J) Scatter plot of rete ridge score vs. age in cellulite and female controls.

Regression lines were drawn separately for each group. (k, l) Elastica van Gieson stained sections show elastic fibers (black) and collagen (red) in cellulite skin. In six out of 25 cellulite specimens, but not in normal control skin, irregularly condensed collagen (arrowheads) in the papillary dermis was observed (k, l). (m, n) Hyaluronic acid staining with biotinylated hyaluronic acid binding protein (red). Representative images of sections from female control (m) and cellulite samples (n) are shown. Bars: 200 µm.

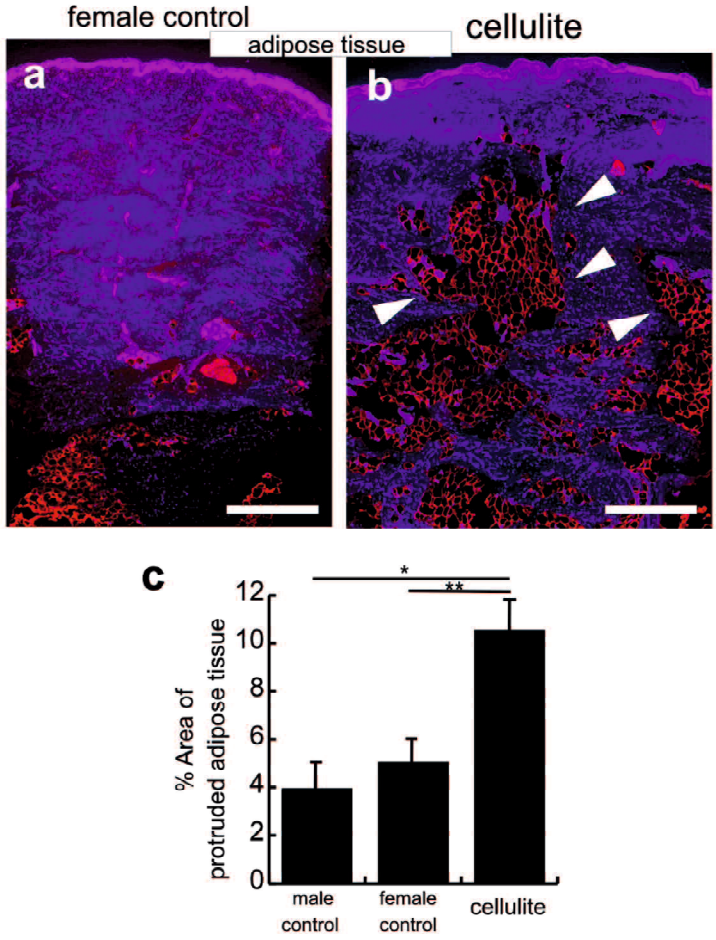

Figure 3-2. Adipose tissue in cellulite

(a, b) Immunohistochemical stainings for perilipin to reveal adipose tissue (red). Co-staining of nuclei was performed using Hoechst 33342. Representative images of female control (a) and cellulite samples (b) are shown. Arrowheads indicate protruded adipose tissue in the dermis. Bars: 1 mm (a, b). (c) The area of protruded adipose tissue was measured in a 4-mm-deep and 3-mm-wide area (below the epidermis). The percentages represent the relative area covered by perilipin-positive adipose tissue and are expressed as mean ± SEM calculated for cellulite (n=24), female control (n=18) and male control (n=4) samples. ** $P<0.01$, * $P<0.05$.

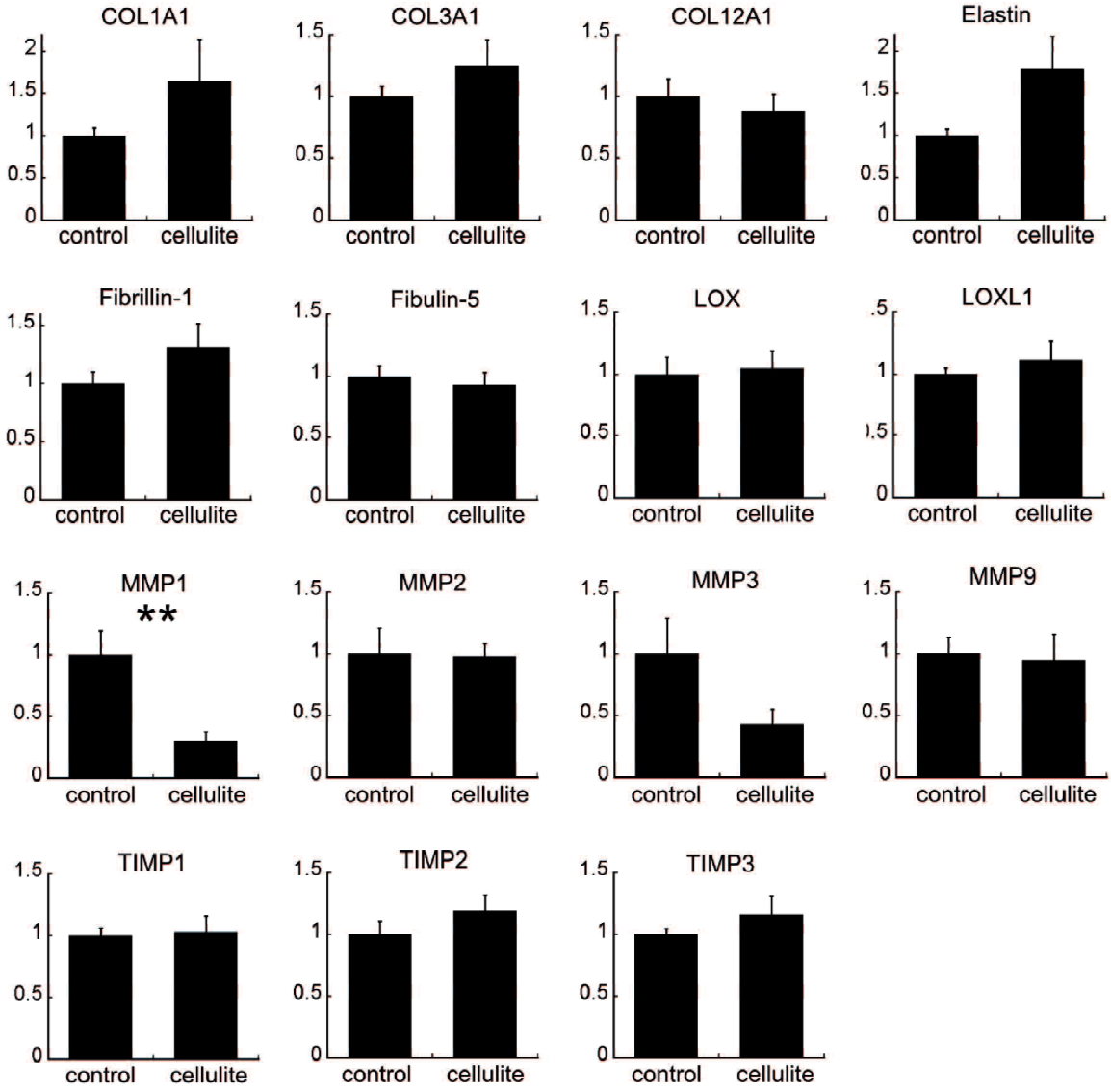

Figure 3-3. qRT-PCR analyses of mRNA expression of major extracellular matrix-related genes

qRT-PCR analyses of mRNA expression of collagens, elastic fiber-related genes, fibulin-5, LOX, LOXL1, MMPs and TIMPs in tissue lysates of cellulite samples compared with female control samples. Results are expressed as fold change in cellulite (n=10) over female control (n=10) for each gene (mean ± SEM). Expression of MMP1 was significantly decreased in cellulite samples, whereas there were no major differences for the other genes. Expression was normalized to GAPDH. **P<0.01.

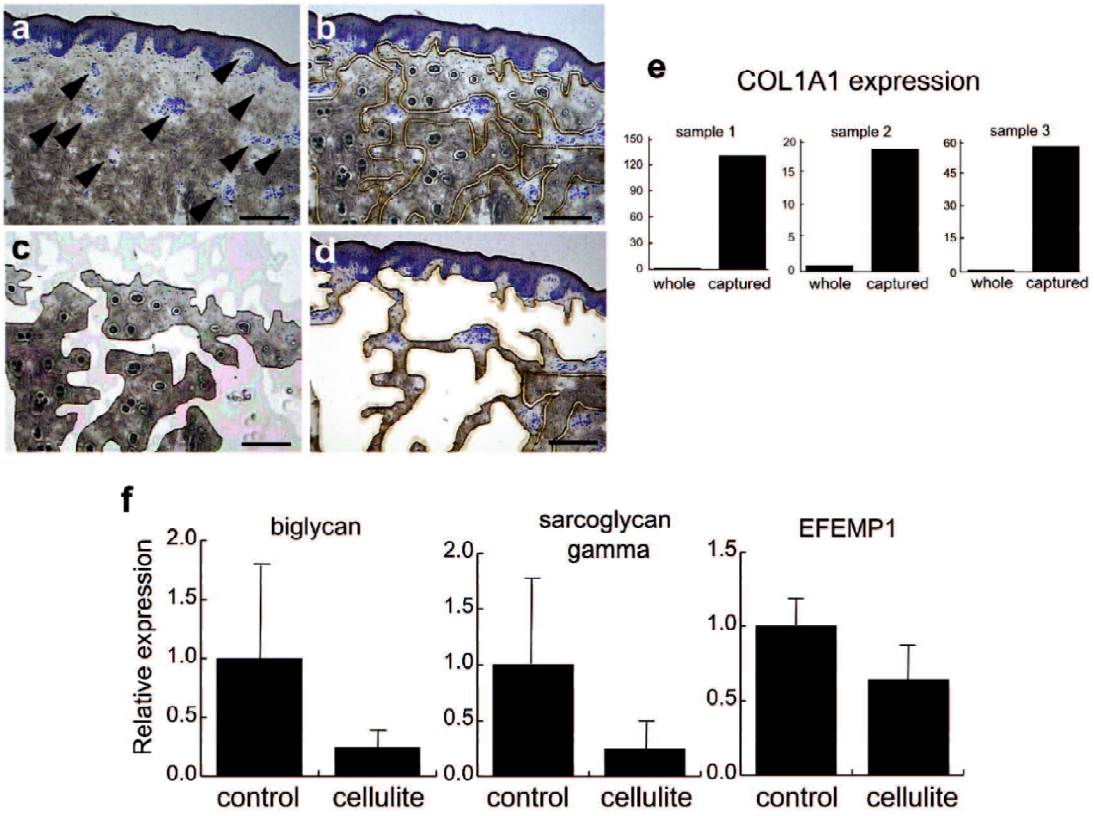

Figure 3-4. Laser capture microdissection of fibroblasts from skin sections and qRT-PCR analyses

Laser capture microdissection of fibroblasts from skin sections. (a–d) LCM of fibroblasts from areas enriched in single cells in the dermis. The same area of a representative skin section was stained before LCM (a), after cutting the areas of interest (b) and after LCM (d). The captured areas of single cells are shown in C. Arrowheads indicate blood vessels and skin appendages which were not captured to avoid contamination by other cell types. Bars: 200 µm (a-d). (e) qRT-PCR analyses for the fibroblast marker COL1A1 in the captured tissue compared with samples from the whole skin region. Results are expressed as fold increase in captured tissue over whole tissue. Expression was normalized to GAPDH. COL1A1 mRNA expression was highly increased in captured tissue compared with whole tissue, indicating selective enrichment of fibroblasts in the LCM-captured tissue. (f) Reduced expression of biglycan (fold change: 0.25, *P*=0.401), sarcoglycan-gamma (fold change: 0.24, *P*=0.381) and EFEMP1(fold change: 0.64, *P*=0.207) in captured fibroblasts from cellulite samples. Results of qRT-PCR are expressed as fold change of input RNA in captured fibroblasts from cellulite (n=5) compared to female control samples (n=5). Results are shown as mean ± SEM. Input was normalized to 18S rRNA.

Table 3.

Top 10 down-regulated and up-regulated gene in cellulite fibroblasts

Down-regulated gene	Ratio cellulite/control	p-value	Up-regulated gene	Ratio cellulite/control	p-value
PDGFRL	0.54	0.081	ACTA2	1.88	0.279
SGCG	0.55	0.014	SLC7A6OS	1.60	0.081
DPF2	0.55	0.089	TTC1	1.55	0.198
OS9	0.56	0.104	AC016831.2	1.46	0.062
ARHGDIB	0.57	0.091	TSPYL5	1.44	0.027
EFEMP1	0.60	0.114	ZFP62	1.42	0.127
BGN	0.61	0.298	CCDC45	1.35	0.012
ERCC1	0.61	0.084	ANKRD36B	1.33	0.067
MMP2	0.61	0.036	ERCC5	1.32	0.199
C1R	0.63	0.148	ATPIF1	1.32	0.125

Top 10 genes are listed as excerpts after that genes were filtered using the following filter settings: Log2 signal >6.4, P-value <0.3, present probe number >8, present probe ratio (present probe number/total probe number) >0.9.

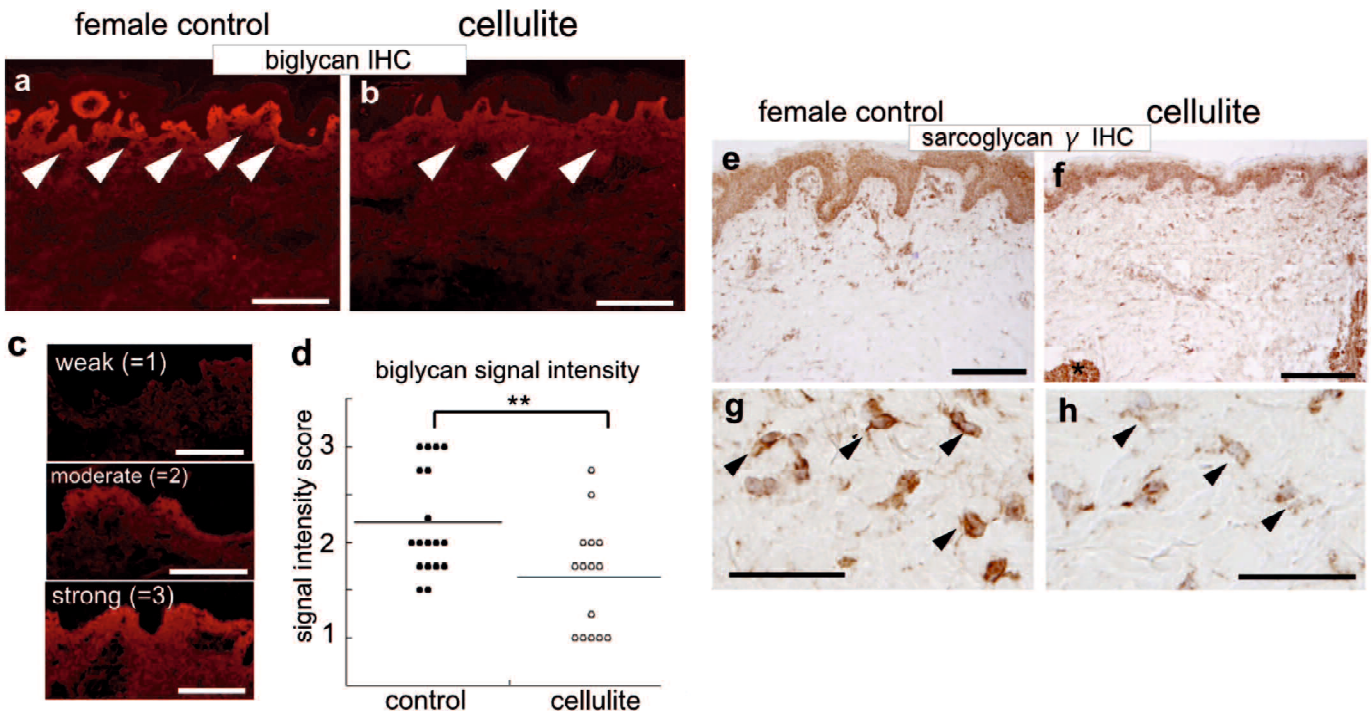

Figure 3-5. Reduced expression of biglycan and sarcoglycan-gamma in cellulite skin

(a, b) Immunohistochemical staining for biglycan. Representative images of sections from female control (a) and cellulite samples (b) are shown. Arrowheads indicate the dermal region underneath the epidermis. Note the decreased biglycan expression in the dermis of the cellulite sample. (c) Representative images corresponding to biglycan signal intensity scores (strong=3, moderate=2, weak=1), used for the image analysis, are shown. (d) Signal intensity scores for biglycan staining in cellulite (n=15) and female control samples (n=18). **P<0.01. (e–h) Representative images of immunostains for sarcoglycan-gamma of female control (e, g) and cellulite samples (f, h). Arrowheads indicate dermal fibroblasts. Asterisk indicates the arrector pili muscle. Nuclear staining with hematoxylin (light blue). Bars: 200 µm in a, b, e, f; 100 µm in c; 50 µm in g, h.

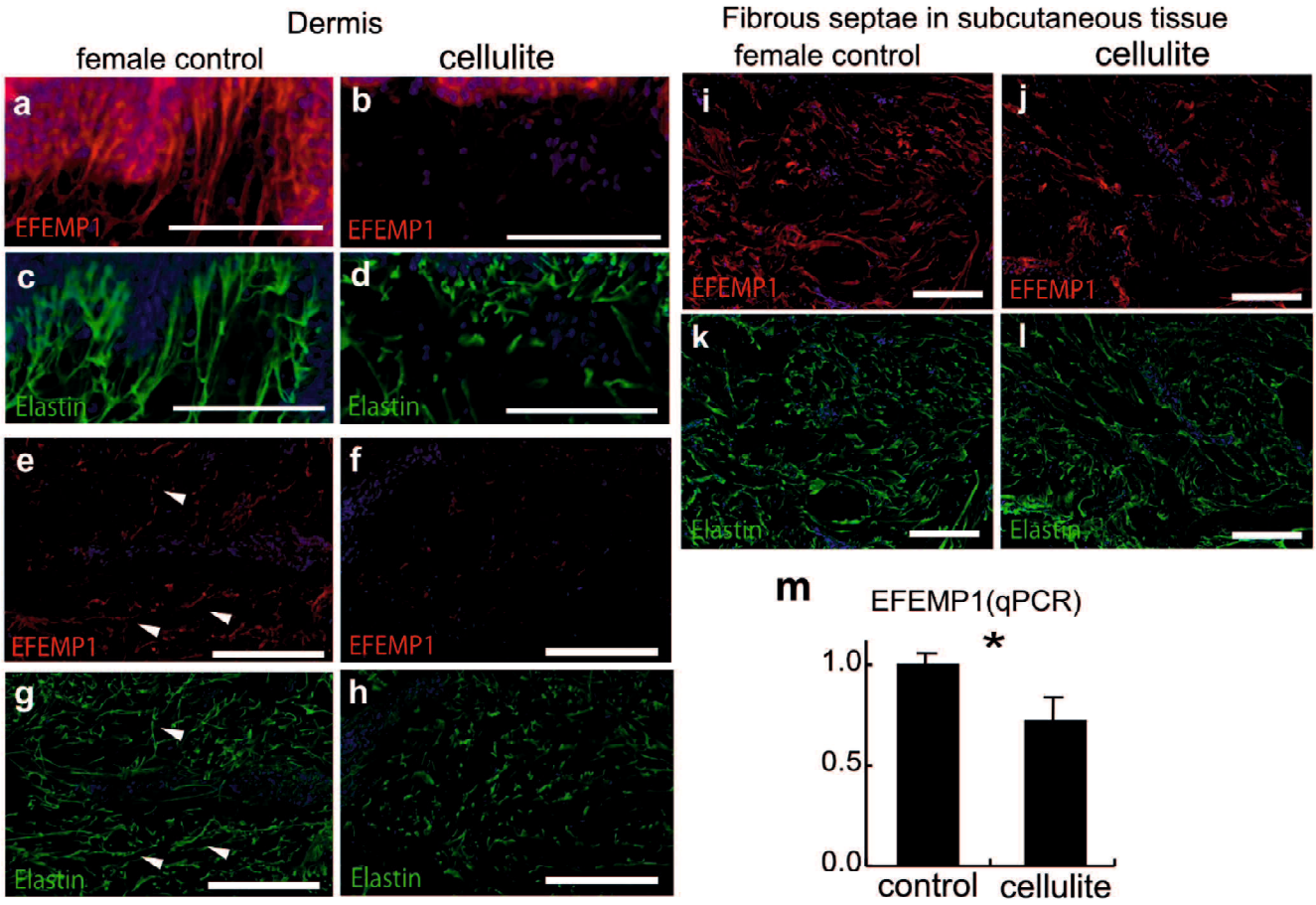

Figure 3-6. Reduced EFEMP1 expression in cellulite

(a–l) Double immunofluorescence stains for EFEMP1 (red) and elastin (green), together with Hoechst nuclear staining. (a–d) Representative images of the basement membrane area and the intersection between the epidermis and the dermis in female control (a, c) and cellulite samples (b, d). (e–h) Representative images of the dermis of female control (e, g) and cellulite samples (f, h). Arrowheads indicate dermal elastic fibers. (i–l) Representative images of fibrous septae in the subcutaneous tissue of female control (i, k) and cellulite samples (j, l) stained for EFEMP1 (i, j) or elastin (k, l). (m) qRT-PCR analyses of EFEMP1 mRNA expression in whole skin lysates from cellulite and female control samples. Results are expressed as fold change in cellulite (n=10) over control samples (n=10 per group). Results are expressed as mean ± SEM. Input was normalized to GAPDH. *P<0.05. Bars: 100 μm in a–d; 200 μm in e–l.

CHAPTER IV:
Summary and conclusion

CHAPTER IV: Summary and conclusion

In CHAPTER II, the role of dermal sheath cells, dermal papilla cells and dermal sheath cup cells in hair morphogenesis and maintenance was investigated. In CHAPTER II.1 the results indicated that CD36-expressing DS cells may modulate blood capillary formation in human hair follicles and may also participate in human hair cycling. Hair thinning in human androgenic alopecia is caused by the miniaturization of hair follicles through affected hair cycling. It can also in animals, such as dogs, and is called alopecia X with notable hair thinning due to disrupted hair cycling with a shortened anagen stage [94]. Although further studies are needed to investigate whether modified CD36 expressing DS cells are observed in human alopecia and alopecia X, the findings of the current study could be used to develop treatments or medicine for alopecia in humans and animals, with a focus on the role of DS cells, which modulate blood capillary formation in hair follicles. Because our results and recent reports [33] indicate that DS cells may have multi-differentiation potential, further studies should be conducted to assess the use of DS cells for cell-based therapy as mesenchymal stem cells.

In CHAPTER II.2 it was indicated that activation of Wnt signaling and spheroid formation synergistically restores hair inducing ability through 'activated' DP spheroids contributing to hair follicle formation. Generated humanized skin with enriched hair

follicles could be a powerful assessment model to understand physiological phenomenon in human, originally indicated by mouse experiments, and also to assess the behavior of cutaneous injected potential cells for cell-based therapy, which is critical to develop cell-based therapy, especially for alopecia. In fact, human DSC cells have been assessed in generated humanized skin, and the injected human cells showed potential for use in cell-based therapy against alopecia.

In summary, the studies in CHAPTER II show several findings that could be applied to develop treatments, especially cell-based therapy for alopecia in humans and animals.

In CHAPTER III, the mechanism underlying cellulite formation was studied. A key finding of our study was the increased protrusion of adipose tissue into the dermis, a reduction of elastic fibers and the thinning of the papillary dermis. These findings suggest the characteristic features of cellulite is due to a reduced function of the dermis to act as a cushion against fat protrusion leading to the outward manifestation of ripples in the skin. Furthermore, decreased EFEMP1, biglycan, sarcoglycan-gamma in cellulite was shown, compared to normal skin. EFEMP1 contributes to the integrity of elastic fibers in the connective tissue of fasciae and the vaginal wall. A lack of EFEMP1 causes inguinal hernias and pelvic prolapse [92, 93]. Hence, mechanisms that decrease EFEMP1 may cause reduced elasticity of the dermis, which leads to fat protrusion and the characteristic

cellulite appearance. EFEMP1 is also expressed in other connective tissue, if the decrease of EFEMP1 is a systemically induced phenomenon, reduced function of connective tissue, other than dermis, may occur. In repeat breeder dairy cows, prolapse of the uterus can occur. The findings obtained in this cellulite study might support the development of preventive methods for that disease.

In this thesis, the mechanisms underlying affected hair by modified hair mesenchymal cells and cellulite formation by modified fibroblasts and dermis were partly delineated. These findings could be used to develop countermeasures against skin diseases in both humans and animals.

References

1. Goldsmith LA. My organ is bigger than your organ. Arch Dermatol. 1990;126(3):301-2. PubMed PMID: 2310204.
2. Sontheimer RD. Skin is not the largest organ. J Invest Dermatol. 2014;134(2):581-2. doi: 10.1038/jid.2013.335. PubMed PMID: 23924902.
3. Potter BS. Bibliographic landmarks in the history of dermatology. J Am Acad Dermatol. 2003;48(6):919-32. doi: 10.1067/mjd.2003.291. PubMed PMID: 12789185.
4. Holubar K, Frankl J. Joseph Plenck (1735-1807). A forerunner of modern European dermatology. J Am Acad Dermatol. 1984;10(2 Pt 1):326-32. PubMed PMID: 6371073.
5. Crissey JT, Parish LC. Two hundred years of dermatology. J Am Acad Dermatol. 1998;39(6):1002-6. doi: 10.1016/s0190-9622(98)70277-4. PubMed PMID: 9843016.
6. Weinstein GD, McCullough JL, Ross P. Cell proliferation in normal epidermis. J Invest Dermatol. 1984;82(6):623-8. doi: 10.1111/1523-1747.ep12261462. PubMed PMID: 6725985.
7. Montagna W, Carlisle K. Structural changes in aging human skin. J Invest Dermatol. 1979;73(1):47-53. doi: 10.1111/1523-1747.ep12532761. PubMed PMID: 448177.
8. Kubo A, Nagao K, Amagai M. Epidermal barrier dysfunction and cutaneous sensitization in atopic diseases. J Clin Invest. 2012;122(2):440-7. doi: 10.1172/JCI57416. PubMed PMID: 22293182; PubMed Central PMCID: PMCPMC3266780.
9. Merad M, Ginhoux F, Collin M. Origin, homeostasis and function of Langerhans cells and other langerin-expressing dendritic cells. Nat Rev Immunol. 2008;8(12):935-47. doi: 10.1038/nri2455. PubMed PMID: 19029989.
10. Kubo A, Nagao K, Yokouchi M, Sasaki H, Amagai M. External antigen uptake by Langerhans cells with reorganization of epidermal tight junction barriers. J Exp Med. 2009;206(13):2937-46. doi: 10.1084/jem.20091527. PubMed PMID: 19995951; PubMed Central PMCID: PMCPMC2806471.
11. Alaluf S, Atkins D, Barrett K, Blount M, Carter N, Heath A. Ethnic variation in melanin content and composition in photoexposed and photoprotected human skin. Pigment Cell Res. 2002;15(2):112-8. doi: 10.1034/j.1600-0749.2002.1o071.x. PubMed PMID: 11936268.
12. Iozumi K, Hoganson GE, Pennella R, Everett MA, Fuller BB. Role of tyrosinase as the determinant of pigmentation in cultured human melanocytes. J Invest Dermatol. 1993;100(6):806-11. doi: 10.1111/1523-1747.ep12476630. PubMed PMID: 8496620.
13. Tajima S, Pinnell SR. Collagen synthesis by human skin fibroblasts in culture: studies of

fibroblasts explanted from papillary and reticular dermis. J Invest Dermatol. 1981;77(5):410-2. doi: 10.1111/1523-1747.ep12494614. PubMed PMID: 7288206.

14. Schonherr E, Beavan LA, Hausser H, Kresse H, Culp LA. Differences in decorin expression by papillary and reticular fibroblasts in vivo and in vitro. Biochem J. 1993;290 (Pt 3):893-9. doi: 10.1042/bj2900893. PubMed PMID: 8457216; PubMed Central PMCID: PMCPMC1132364.
15. Izumi T, Tajima S, Nishikawa T. Differential expression of alpha 1 and alpha 2 chains of type VI collagen in the upper, middle, and lower dermal fibroblasts in vitro. J Biochem. 1995;117(5):1004-7. doi: 10.1093/oxfordjournals.jbchem.a124798. PubMed PMID: 8586611.
16. Mine S, Fortunel NO, Pageon H, Asselineau D. Aging alters functionally human dermal papillary fibroblasts but not reticular fibroblasts: a new view of skin morphogenesis and aging. PLoS One. 2008;3(12):e4066. doi: 10.1371/journal.pone.0004066. PubMed PMID: 19115004; PubMed Central PMCID: PMCPMC2605251.
17. Sorrell JM, Caplan AI. Fibroblast heterogeneity: more than skin deep. J Cell Sci. 2004;117(Pt 5):667-75. doi: 10.1242/jcs.01005. PubMed PMID: 14754903.
18. Quan T, Shao Y, He T, Voorhees JJ, Fisher GJ. Reduced expression of connective tissue growth factor (CTGF/CCN2) mediates collagen loss in chronologically aged human skin. J Invest Dermatol. 2010;130(2):415-24. doi: 10.1038/jid.2009.224. PubMed PMID: 19641518; PubMed Central PMCID: PMCPMC2877594.
19. Braverman IM, Fonferko E. Studies in cutaneous aging: I. The elastic fiber network. J Invest Dermatol. 1982;78(5):434-43. doi: 10.1111/1523-1747.ep12507866. PubMed PMID: 7069221.
20. Ezure T, Hosoi J, Amano S, Tsuchiya T. Sagging of the cheek is related to skin elasticity, fat mass and mimetic muscle function. Skin Res Technol. 2009;15(3):299-305. doi: 10.1111/j.1600-0846.2009.00364.x. PubMed PMID: 19624426.
21. Braverman IM. Ultrastructure and organization of the cutaneous microvasculature in normal and pathologic states. J Invest Dermatol. 1989;93(2 Suppl):2S-9S. doi: 10.1111/1523-1747.ep12580893. PubMed PMID: 2666519.
22. Skobe M, Detmar M. Structure, function, and molecular control of the skin lymphatic system. J Investig Dermatol Symp Proc. 2000;5(1):14-9. doi: 10.1046/j.1087-0024.2000.00001.x. PubMed PMID: 11147669.
23. Segura S, Requena L. Anatomy and histology of normal subcutaneous fat, necrosis of adipocytes, and classification of the panniculitides. Dermatol Clin. 2008;26(4):419-24, v. doi: 10.1016/j.det.2008.05.011. PubMed PMID: 18793973.
24. Sato K, Dobson RL. Regional and individual variations in the function of the human

eccrine sweat gland. J Invest Dermatol. 1970;54(6):443-9. doi: 10.1111/1523-1747.ep12259272. PubMed PMID: 5446389.

25. Otberg N, Richter H, Schaefer H, Blume-Peytavi U, Sterry W, Lademann J. Variations of hair follicle size and distribution in different body sites. J Invest Dermatol. 2004;122(1):14-9. doi: 10.1046/j.0022-202X.2003.22110.x. PubMed PMID: 14962084.
26. Crisan M, Yap S, Casteilla L, Chen CW, Corselli M, Park TS, et al. A perivascular origin for mesenchymal stem cells in multiple human organs. Cell Stem Cell. 2008;3(3):301-13. doi: 10.1016/j.stem.2008.07.003. PubMed PMID: 18786417.
27. Paquet-Fifield S, Schluter H, Li A, Aitken T, Gangatirkar P, Blashki D, et al. A role for pericytes as microenvironmental regulators of human skin tissue regeneration. J Clin Invest. 2009;119(9):2795-806. doi: 10.1172/JCI38535. PubMed PMID: 19652362; PubMed Central PMCID: PMCPMC2735900.
28. Hinz B, Phan SH, Thannickal VJ, Galli A, Bochaton-Piallat ML, Gabbiani G. The myofibroblast: one function, multiple origins. Am J Pathol. 2007;170(6):1807-16. doi: 10.2353/ajpath.2007.070112. PubMed PMID: 17525249; PubMed Central PMCID: PMCPMC1899462.
29. Hardy MH. The secret life of the hair follicle. Trends Genet. 1992;8(2):55-61. doi: 10.1016/0168-9525(92)90350-d. PubMed PMID: 1566372.
30. Ohyama M, Zheng Y, Paus R, Stenn KS. The mesenchymal component of hair follicle neogenesis: background, methods and molecular characterization. Exp Dermatol. 2010;19(2):89-99. doi: 10.1111/j.1600-0625.2009.00935.x. PubMed PMID: 19650868.
31. Driskell RR, Lichtenberger BM, Hoste E, Kretzschmar K, Simons BD, Charalambous M, et al. Distinct fibroblast lineages determine dermal architecture in skin development and repair. Nature. 2013;504(7479):277-81. doi: 10.1038/nature12783. PubMed PMID: 24336287; PubMed Central PMCID: PMCPMC3868929.
32. Driskell RR, Clavel C, Rendl M, Watt FM. Hair follicle dermal papilla cells at a glance. J Cell Sci. 2011;124(Pt 8):1179-82. doi: 10.1242/jcs.082446. PubMed PMID: 21444748; PubMed Central PMCID: PMCPMC3115771.
33. Biernaskie J, Paris M, Morozova O, Fagan BM, Marra M, Pevny L, et al. SKPs derive from hair follicle precursors and exhibit properties of adult dermal stem cells. Cell Stem Cell. 2009;5(6):610-23. doi: 10.1016/j.stem.2009.10.019. PubMed PMID: 19951689; PubMed Central PMCID: PMCPMC2828150.
34. Yu H, Kumar SM, Kossenkov AV, Showe L, Xu X. Stem cells with neural crest characteristics derived from the bulge region of cultured human hair follicles. J Invest Dermatol. 2010;130(5):1227-36. doi: 10.1038/jid.2009.322. PubMed PMID: 19829300; PubMed Central PMCID: PMCPMC3050599.

35. Festa E, Fretz J, Berry R, Schmidt B, Rodeheffer M, Horowitz M, et al. Adipocyte lineage cells contribute to the skin stem cell niche to drive hair cycling. Cell. 2011;146(5):761-71. doi: 10.1016/j.cell.2011.07.019. PubMed PMID: 21884937; PubMed Central PMCID: PMCPMC3298746.
36. Gudjonsson JE, Johnston A, Dyson M, Valdimarsson H, Elder JT. Mouse models of psoriasis. J Invest Dermatol. 2007;127(6):1292-308. doi: 10.1038/sj.jid.5700807. PubMed PMID: 17429444.
37. Moniaga CS, Egawa G, Kawasaki H, Hara-Chikuma M, Honda T, Tanizaki H, et al. Flaky tail mouse denotes human atopic dermatitis in the steady state and by topical application with Dermatophagoides pteronyssinus extract. Am J Pathol. 2010;176(5):2385-93. doi: 10.2353/ajpath.2010.090957. PubMed PMID: 20304960; PubMed Central PMCID: PMCPMC2861103.
38. Matsumura H, Mohri Y, Binh NT, Morinaga H, Fukuda M, Ito M, et al. Hair follicle aging is driven by transepidermal elimination of stem cells via COL17A1 proteolysis. Science. 2016;351(6273):aad4395. doi: 10.1126/science.aad4395. PubMed PMID: 26912707.
39. Horne KA, Jahoda CA. Restoration of hair growth by surgical implantation of follicular dermal sheath. Development. 1992;116(3):563-71. PubMed PMID: 1289054.
40. McElwee KJ, Kissling S, Wenzel E, Huth A, Hoffmann R. Cultured peribulbar dermal sheath cells can induce hair follicle development and contribute to the dermal sheath and dermal papilla. J Invest Dermatol. 2003;121(6):1267-75. doi: 10.1111/j.1523-1747.2003.12568.x. PubMed PMID: 14675169.
41. Matsuzaki T, Inamatsu M, Yoshizato K. The upper dermal sheath has a potential to regenerate the hair in the rat follicular epidermis. Differentiation. 1996;60(5):287-97. doi: 10.1046/j.1432-0436.1996.6050287.x. PubMed PMID: 8855372.
42. Reynolds AJ, Lawrence C, Cserhalmi-Friedman PB, Christiano AM, Jahoda CA. Trans-gender induction of hair follicles. Nature. 1999;402(6757):33-4. doi: 10.1038/46938. PubMed PMID: 10573414.
43. Tobin DJ, Gunin A, Magerl M, Handijski B, Paus R. Plasticity and cytokinetic dynamics of the hair follicle mesenchyme: implications for hair growth control. J Invest Dermatol. 2003;120(6):895-904. doi: 10.1046/j.1523-1747.2003.12237.x. PubMed PMID: 12787113.
44. Rahmani W, Abbasi S, Hagner A, Raharjo E, Kumar R, Hotta A, et al. Hair follicle dermal stem cells regenerate the dermal sheath, repopulate the dermal papilla, and modulate hair type. Developmental cell. 2014;31(5):543-58. doi: 10.1016/j.devcel.2014.10.022. PubMed PMID: 25465495.
45. Jindo T, Tsuboi R, Takamori K, Ogawa H. Local injection of hepatocyte growth

factor/scatter factor (HGF/SF) alters cyclic growth of murine hair follicles. J Invest Dermatol. 1998;110(4):338-42. doi: 10.1046/j.1523-1747.1998.00144.x. PubMed PMID: 9540971.

46. Bussolino F, Di Renzo MF, Ziche M, Bocchietto E, Olivero M, Naldini L, et al. Hepatocyte growth factor is a potent angiogenic factor which stimulates endothelial cell motility and growth. J Cell Biol. 1992;119(3):629-41. doi: 10.1083/jcb.119.3.629. PubMed PMID: 1383237; PubMed Central PMCID: PMCPMC2289675.
47. Febbraio M, Hajjar DP, Silverstein RL. CD36: a class B scavenger receptor involved in angiogenesis, atherosclerosis, inflammation, and lipid metabolism. J Clin Invest. 2001;108(6):785-91. doi: 10.1172/JCI14006. PubMed PMID: 11560944; PubMed Central PMCID: PMCPMC200943.
48. Yoshida Y, Kajiya K, Kishimoto J, Detmar M. Quantitative histological analyses and transcriptional profiling reveal structural and molecular changes of the dermal extracellular matrix in cellulite. J Dermatol Sci. 2018;92(1):6-9. doi: 10.1016/j.jdermsci.2018.06.010. PubMed PMID: 30041986.
49. Oh JW, Kloepper J, Langan EA, Kim Y, Yeo J, Kim MJ, et al. A Guide to Studying Human Hair Follicle Cycling In Vivo. J Invest Dermatol. 2016;136(1):34-44. doi: 10.1038/JID.2015.354. PubMed PMID: 26763421; PubMed Central PMCID: PMCPMC4785090.
50. Schmittgen TD, Livak KJ. Analyzing real-time PCR data by the comparative C(T) method. Nat Protoc. 2008;3(6):1101-8. PubMed PMID: 18546601.
51. Dvorak HF, Brown LF, Detmar M, Dvorak AM. Vascular permeability factor/vascular endothelial growth factor, microvascular hyperpermeability, and angiogenesis. Am J Pathol. 1995;146(5):1029-39. PubMed PMID: 7538264; PubMed Central PMCID: PMCPMC1869291.
52. Yano K, Brown LF, Detmar M. Control of hair growth and follicle size by VEGF-mediated angiogenesis. J Clin Invest. 2001;107(4):409-17. doi: 10.1172/JCI11317. PubMed PMID: 11181640; PubMed Central PMCID: PMCPMC199257.
53. Mecklenburg L, Tobin DJ, Muller-Rover S, Handjiski B, Wendt G, Peters EM, et al. Active hair growth (anagen) is associated with angiogenesis. J Invest Dermatol. 2000;114(5):909-16. doi: 10.1046/j.1523-1747.2000.00954.x. PubMed PMID: 10771470.
54. Dvorak HF. Angiogenesis: update 2005. J Thromb Haemost. 2005;3(8):1835-42. doi: 10.1111/j.1538-7836.2005.01361.x. PubMed PMID: 16102050.
55. Montagna W, Ellis RA. Histology and cytochemistry of human skin. XIII. The blood supply of the hair follicle. J Natl Cancer Inst. 1957;19(3):451-63. doi: 10.1093/jnci/19.3.451. PubMed PMID: 13502726.

56. Ellis RA, Moretti G. Vascular patterns associated with categen hair follicles in the human scalp. Ann N Y Acad Sci. 1959;83:448-57. PubMed PMID: 13820052.
57. Yano K, Brown LF, Lawler J, Miyakawa T, Detmar M. Thrombospondin-1 plays a critical role in the induction of hair follicle involution and vascular regression during the catagen phase. J Invest Dermatol. 2003;120(1):14-9. doi: 10.1046/j.1523-1747.2003.12045.x. PubMed PMID: 12535193.
58. Wu JJ, Zhu TY, Lu YG, Liu RQ, Mai Y, Cheng B, et al. Hair follicle reformation induced by dermal papilla cells from human scalp skin. Arch Dermatol Res. 2006;298(4):183-90. doi: 10.1007/s00403-006-0686-9. PubMed PMID: 16897077.
59. Inoue K, Kato H, Sato T, Osada A, Aoi N, Suga H, et al. Evaluation of animal models for the hair-inducing capacity of cultured human dermal papilla cells. Cells Tissues Organs. 2009;190(2):102-10. doi: 10.1159/000178021. PubMed PMID: 19033718.
60. Ohyama M, Kobayashi T, Sasaki T, Shimizu A, Amagai M. Restoration of the intrinsic properties of human dermal papilla in vitro. J Cell Sci. 2012;125(Pt 17):4114-25. doi: 10.1242/jcs.105700. PubMed PMID: 22623722.
61. Inamatsu M, Matsuzaki T, Iwanari H, Yoshizato K. Establishment of rat dermal papilla cell lines that sustain the potency to induce hair follicles from afollicular skin. J Invest Dermatol. 1998;111(5):767-75. doi: 10.1046/j.1523-1747.1998.00382.x. PubMed PMID: 9804336.
62. Kishimoto J, Burgeson RE, Morgan BA. Wnt signaling maintains the hair-inducing activity of the dermal papilla. Genes Dev. 2000;14(10):1181-5. PubMed PMID: 10817753; PubMed Central PMCID: PMCPMC316619.
63. Naujok O, Lentes J, Diekmann U, Davenport C, Lenzen S. Cytotoxicity and activation of the Wnt/beta-catenin pathway in mouse embryonic stem cells treated with four GSK3 inhibitors. BMC Res Notes. 2014;7:273. doi: 10.1186/1756-0500-7-273. PubMed PMID: 24779365; PubMed Central PMCID: PMCPMC4008422.
64. Higgins CA, Chen JC, Cerise JE, Jahoda CA, Christiano AM. Microenvironmental reprogramming by three-dimensional culture enables dermal papilla cells to induce de novo human hair-follicle growth. Proc Natl Acad Sci U S A. 2013;110(49):19679-88. doi: 10.1073/pnas.1309970110. PubMed PMID: 24145441; PubMed Central PMCID: PMCPMC3856847.
65. Botchkarev VA, Kishimoto J. Molecular control of epithelial-mesenchymal interactions during hair follicle cycling. J Investig Dermatol Symp Proc. 2003;8(1):46-55. doi: 10.1046/j.1523-1747.2003.12171.x. PubMed PMID: 12894994.
66. Driskell RR, Giangreco A, Jensen KB, Mulder KW, Watt FM. Sox2-positive dermal papilla cells specify hair follicle type in mammalian epidermis. Development. 2009;136(16):2815-

23. doi: 10.1242/dev.038620. PubMed PMID: 19605494; PubMed Central PMCID: PMCPMC2730408.

67. Lee LF, Jiang TX, Garner W, Chuong CM. A simplified procedure to reconstitute hair-producing skin. Tissue Eng Part C Methods. 2011;17(4):391-400. doi: 10.1089/ten.TEC.2010.0477. PubMed PMID: 21034159; PubMed Central PMCID: PMCPMC3065728.

68. Soma T, Fujiwara S, Shirakata Y, Hashimoto K, Kishimoto J. Hair-inducing ability of human dermal papilla cells cultured under Wnt/beta-catenin signalling activation. Exp Dermatol. 2012;21(4):307-9. doi: 10.1111/j.1600-0625.2012.01458.x. PubMed PMID: 22417309.

69. Amin N, Vincan E. The Wnt signaling pathways and cell adhesion. Front Biosci (Landmark Ed). 2012;17:784-804. PubMed PMID: 22201774.

70. Wu X, Scott L, Jr., Washenik K, Stenn K. Full-thickness skin with mature hair follicles generated from tissue culture expanded human cells. Tissue Eng Part A. 2014;20(23-24):3314-21. doi: 10.1089/ten.TEA.2013.0759. PubMed PMID: 25074625.

71. Smalls LK, Lee CY, Whitestone J, Kitzmiller WJ, Wickett RR, Visscher MO. Quantitative model of cellulite: three-dimensional skin surface topography, biophysical characterization, and relationship to human perception. J Cosmet Sci. 2005;56(2):105-20. PubMed PMID: 15868063.

72. Mirrashed F, Sharp JC, Krause V, Morgan J, Tomanek B. Pilot study of dermal and subcutaneous fat structures by MRI in individuals who differ in gender, BMI, and cellulite grading. Skin Res Technol. 2004;10(3):161-8. PubMed PMID: 15225265.

73. Callaghan T, Wilhelm KP. An examination of non-invasive imaging techniques in the analysis and review of cellulite. J Cosmet Sci. 2005;56(6):379-93. PubMed PMID: 16538294.

74. Rossi AB, Vergnanini AL. Cellulite: a review. J Eur Acad Dermatol Venereol. 2000;14(4):251-62. PubMed PMID: 11204512.

75. Querleux B, Cornillon C, Jolivet O, Bittoun J. Anatomy and physiology of subcutaneous adipose tissue by in vivo magnetic resonance imaging and spectroscopy: relationships with sex and presence of cellulite. Skin Res Technol. 2002;8(2):118-24. PubMed PMID: 12060477.

76. Pierard GE, Nizet JL, Pierard-Franchimont C. Cellulite: from standing fat herniation to hypodermal stretch marks. Am J Dermatopathol. 2000;22(1):34-7. PubMed PMID: 10698214.

77. Irizarry RA, Hobbs B, Collin F, Beazer-Barclay YD, Antonellis KJ, Scherf U, et al. Exploration, normalization, and summaries of high density oligonucleotide array probe

level data. Biostatistics (Oxford, England). 2003;4(2):249-64. PubMed PMID: 12925520.

78. Greenberg AS, Egan JJ, Wek SA, Garty NB, Blanchette-Mackie EJ, Londos C. Perilipin, a major hormonally regulated adipocyte-specific phosphoprotein associated with the periphery of lipid storage droplets. J Biol Chem. 1991;266(17):11341-6. PubMed PMID: 2040638.

79. Ezure T, Amano S. Increased subcutaneous adipose tissue impairs dermal function in diet-induced obese mice. Exp Dermatol. 19(10):878-82. PubMed PMID: 19758317.

80. Ezure T, Amano S. Negative regulation of dermal fibroblasts by enlarged adipocytes through release of free fatty acids. J Invest Dermatol. 131(10):2004-9. PubMed PMID: 21697886.

81. Smith LT, Holbrook KA, Madri JA. Collagen types I, III, and V in human embryonic and fetal skin. Am J Anat. 1986;175(4):507-21. PubMed PMID: 3521252.

82. Wagenseil JE, Mecham RP. New insights into elastic fiber assembly. Birth Defects Res C Embryo Today. 2007;81(4):229-40. PubMed PMID: 18228265.

83. Hocking AM, Shinomura T, McQuillan DJ. Leucine-rich repeat glycoproteins of the extracellular matrix. Matrix Biol. 1998;17(1):1-19. PubMed PMID: 9628249.

84. Bianco P, Fisher LW, Young MF, Termine JD, Robey PG. Expression and localization of the two small proteoglycans biglycan and decorin in developing human skeletal and non-skeletal tissues. J Histochem Cytochem. 1990;38(11):1549-63. PubMed PMID: 2212616.

85. Xu T, Bianco P, Fisher LW, Longenecker G, Smith E, Goldstein S, et al. Targeted disruption of the biglycan gene leads to an osteoporosis-like phenotype in mice. Nat Genet. 1998;20(1):78-82. PubMed PMID: 9731537.

86. Corsi A, Xu T, Chen XD, Boyde A, Liang J, Mankani M, et al. Phenotypic effects of biglycan deficiency are linked to collagen fibril abnormalities, are synergized by decorin deficiency, and mimic Ehlers-Danlos-like changes in bone and other connective tissues. J Bone Miner Res. 2002;17(7):1180-9. PubMed PMID: 12102052.

87. Sandona D, Betto R. Sarcoglycanopathies: molecular pathogenesis and therapeutic prospects. Expert Rev Mol Med. 2009;11:e28. PubMed PMID: 19781108.

88. Hack AA, Ly CT, Jiang F, Clendenin CJ, Sigrist KS, Wollmann RL, et al. Gamma-sarcoglycan deficiency leads to muscle membrane defects and apoptosis independent of dystrophin. J Cell Biol. 1998;142(5):1279-87. PubMed PMID: 9732288.

89. Sasaoka T, Imamura M, Araishi K, Noguchi S, Mizuno Y, Takagoshi N, et al. Pathological analysis of muscle hypertrophy and degeneration in muscular dystrophy in gamma-sarcoglycan-deficient mice. Neuromuscul Disord. 2003;13(3):193-206. PubMed PMID: 12609501.

90. de Vega S, Iwamoto T, Yamada Y. Fibulins: multiple roles in matrix structures and tissue

functions. Cell Mol Life Sci. 2009;66(11-12):1890-902. PubMed PMID: 19189051.

91. Timpl R, Sasaki T, Kostka G, Chu ML. Fibulins: a versatile family of extracellular matrix proteins. Nat Rev Mol Cell Biol. 2003;4(6):479-89. PubMed PMID: 12778127.

92. McLaughlin PJ, Bakall B, Choi J, Liu Z, Sasaki T, Davis EC, et al. Lack of fibulin-3 causes early aging and herniation, but not macular degeneration in mice. Hum Mol Genet. 2007;16(24):3059-70. PubMed PMID: 17872905.

93. Rahn DD, Acevedo JF, Roshanravan S, Keller PW, Davis EC, Marmorstein LY, et al. Failure of pelvic organ support in mice deficient in fibulin-3. Am J Pathol. 2009;174(1):206-15. PubMed PMID: 19095964.

94. Muntener T, Schuepbach-Regula G, Frank L, Rufenacht S, Welle MM. Canine noninflammatory alopecia: a comprehensive evaluation of common and distinguishing histological characteristics. Vet Dermatol. 2012;23(3):206-e44. doi: 10.1111/j.1365-3164.2012.01049.x. PubMed PMID: 22575019.

95. Hiroshi Shimizu (2009). Atarashii Hifukagaku (Textbook of modern dermatology), Tokyo: Nakayama Shoten.

List of publications

Main papers listed in the thesis:

[1] Y. Yoshida, T. Soma, J. Kishimoto, Characterization of human dermal sheath cells reveals CD36-expressing perivascular cells associated with capillary blood vessel formation in hair follicles, Biochem Biophys Res Commun, 516-3 (2019) 945-950.

[2] Y. Yoshida, T. Soma, T. Matsuzaki, J. Kishimoto, Wnt activator CHIR99021-stimulated human dermal papilla spheroids contribute to hair follicle formation and production of reconstituted follicle-enriched human skin, Biochem Biophys Res Commun, 516-3 (2019) 599-605.

Related paper listed in the thesis:

[3] Y. Yoshida, K. Kajiya, J. Kishimoto, M. Detmar, Quantitative histological analyses and transcriptional profiling reveal structural and molecular changes of the dermal extracellular matrix in cellulite, J Dermatol Sci, 92 (2018) 6-9.

Acknowledgements

I am deeply grateful to emeritus Prof. Katsutoshi Yoshizato (Faculty of Science, Hiroshima Univ.), emeritus Prof. Hisato Kondoh (Graduate school of Frontier Biosciences, Osaka Univ.) and great their laboratory members. They had educated me what amazing molecular systems life organisms have and how fascinating and exciting molecular biological studies to solve the complexity are.

I am deeply grateful to Prof. Michael Detmar (Institute of Pharmaceutical Sciences, ETH Zurich), Dr. Jiro Kishimoto (Shiseido Research Center) and all their laboratory members. They had enlightened me about how to fulfill the research objectives by sharp and essential research plan, and how to develop the results from basic science to translational research.

I am deeply grateful to Prof. Yoshiaki Yamano (Faculty of Agriculture, Joint Department of Veterinary medicine, Tottori Univ.) who is a chief supervisor for my doctoral thesis. He had enlightened me about essential manners and things which academic scientist should have, through preparation of the manuscript for my doctoral thesis. I am deeply grateful to Lecturer Masashi Higuchi, Prof. Takehito Morita, Prof. Yoshiaki Hikasa (Faculty of Agriculture, Joint Department of Veterinary medicine, Tottori Univ.) and Prof. Akikazu Fujita (Joint faculty of veterinary medicine, Kagoshima Univ.)

for critical reading of the manuscript for my doctoral thesis as assistant supervisors.

And of course, I am deeply grateful to all my family. Specially my parents have strongly supported me anytime especially during university and graduated university. My wife and children support and refresh me all the time. I would like to give many thanks to them as closing sentence.